sustainability

MDPI

Review

A Review on Application of Biochar in the Removal of Pharmaceutical Pollutants through Adsorption and Persulfate-Based AOPs

Ziyang Kang [1], Xigai Jia [1], Yuchen Zhang [1], Xiaoxuan Kang [1], Ming Ge [1], Dong Liu [1], Chongqing Wang [2,*] and Zhangxing He [1,3,*]

[1] College of Chemical Engineering, North China University of Science and Technology, Tangshan 063210, China
[2] School of Chemical Engineering, Zhengzhou University, Zhengzhou 450001, China
[3] Tangshan Sanyou Group Co., Ltd., Tangshan 063305, China
* Correspondence: zilangwang@126.com (C.W.); zxhe@ncst.edu.cn (Z.H.)

Abstract: Increasing quantities of pharmaceutical pollutants have been found in aquatic ecosystems. The treatment of pharmaceutical pollutants has been a major task that people have been committed to in recent years. The removal of pharmaceutical pollutants can be achieved by adsorption and advanced oxidation processes (AOPs). Compared with other carbon materials, biochar has a strong adsorption capacity and persulfate activation ability, and more importantly, biochar is cheap and easy to obtain; thus, it has higher economic benefits. This study firstly reviews the application of biochar in the removal of drugs (tetracycline (TC), sulfamethoxazole (SMX), acetaminophen (ACT), cephalexin (CPX), levofloxacin (LEV), etc.) through adsorption and persulfate-based AOPs. In addition, we summarize the adsorption mechanism of biochar for various pharmaceutical pollutants and the main attack sites on different pharmaceutical pollutants in persulfate-based AOPs catalyzed by biochar. Finally, the challenges and prospects of biochar with respect to the removal of pharmaceutical pollutants are put forward.

Keywords: biochar; pharmaceutical pollutants; adsorption; persulfate; removal mechanism

Citation: Kang, Z.; Jia, X.; Zhang, Y.; Kang, X.; Ge, M.; Liu, D.; Wang, C.; He, Z. A Review on Application of Biochar in the Removal of Pharmaceutical Pollutants through Adsorption and Persulfate-Based AOPs. *Sustainability* **2022**, *14*, 10128. https://doi.org/10.3390/su141610128

Academic Editor: Lakshmanakumar Kinthada

Received: 22 June 2022
Accepted: 12 August 2022
Published: 16 August 2022

1. Introduction

Energy consumption and environmental pollution have always been a difficult problem in the world [1–3]. Due to the rapid development of society, the demand for energy is increasing, which also enhances the dependence on green energy, and new redox batteries can help reduce the energy burden [4–6]. An important aspect of environmental pollution is the pollution of the aquatic environment by drugs. Drugs are widely used around the world to protect humans and animals from various diseases. Specifically, the representative drugs in this case include tetracycline (TC), sulfamethoxazole (SMX), acetaminophen (ACT), cephalexin (CPX), levofloxacin (LEV), etc. [7,8]. The worldwide consumption of antibacterial drugs increased by as much as 65% between 2000 and 2015, from 21.1 billion doses in 2000 to 34.8 billion in 2015. It is estimated that the consumption of global antibiotics in 2030 will be 200% higher than the 42 billion defined daily doses in 2015 [9]. In fact, many drugs are not completely metabolized by humans and animals, and consequently enter the ecological environment through various routes. Figure 1 shows the sources and transfer pathways of drugs in the aquatic environment [10]. On the one hand, drug residues in water and food will accumulate through the food chain for a long time, and then have a potential impact on human health. For example, a long-term accumulation of TC can inhibit children's development and bone growth. On the other hand, after drug residues enter the aquatic environment, drug-resistant bacteria will be induced, which will adversely affect the ecosystem and destroy the ecological balance [9,11]. Both of these effects seriously

threaten environmental safety and public health [12]. Therefore, it is crucial to remove pharmaceutical pollutants from the aquatic environment as soon as possible.

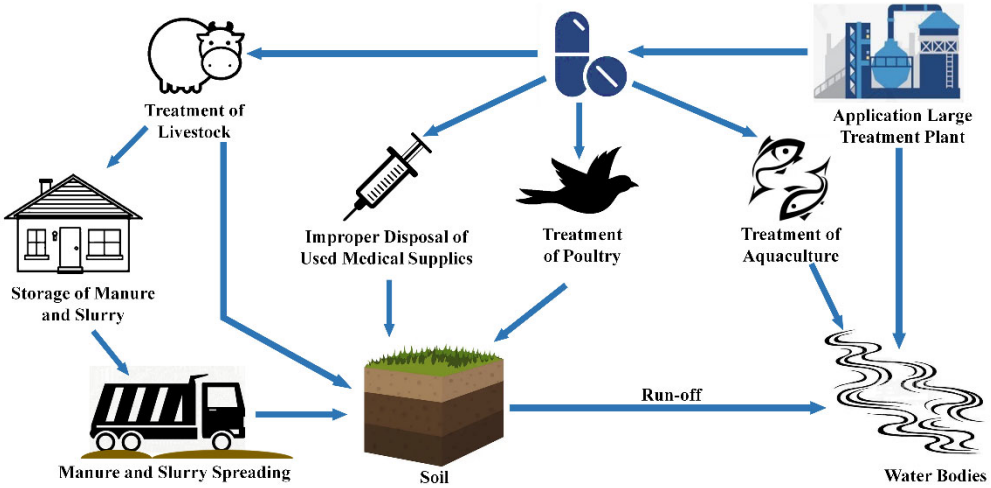

Figure 1. Sources and transfer pathways of drug residues in aquatic environment.

Various strategies, such as physical treatment, chemical treatment, and biological treatment can be used to remove pharmaceutical pollutants [13]. Most drugs have an inhibitory effect on bacterial activity, so the removal efficiency of biological treatment is low [14]. Since the concentration of most pharmaceutical pollutants is at the μg/L level, adsorption technology has the advantages of low cost, strong reproducibility, and high efficiency, which in turn allows it to be an effective method to treat low-concentration pharmaceutical pollutants [15]. In addition to this, research on the removal of pharmaceutical pollutants by advanced oxidation methods (AOPs) has attracted extensive attention [16]. Compared with other AOPs, persulfate-based AOPs have higher oxidizing properties, better selectivity, and no secondary pollution [17]. Therefore, the application of persulfate-based AOPs is also an efficient and economical method for the removal of pharmaceutical pollutants.

Carbon-based materials, such as activated carbon [18], biochar [19], carbon nanotubes [20], and reduced graphene oxide [21], are widely used in the removal of pharmaceutical pollutants through adsorption and persulfate-based AOPs. Among them, biochar prepared from agricultural by-products, sewage sludge, animal manure, and other wastes is a feasible option [22–24]. Biochar has many special advantages, such as a low cost, environmental friendliness, a porous structure, and abundant functional groups (e.g., –OH, –COOH and $–NH_2$), and it is widely considered as a next generation of functional carbon material [25]. Zhang et al. [26] used biochar activated by boric acid to remove sulfadiazine by adsorption, and the adsorption efficiency of sulfadiazine could reach more than 90%, indicating that this material was a promising porous adsorbent, which could effectively remove sulfadiazine and achieve practical applications. It further confirmed the important roles of biochar and modified biochar as adsorbents for the removal of pharmaceutical pollutants. Fang et al. [27] have proposed a possible mechanism for the activation of persulfate by biochar. Persistent free radicals and oxygen-functional groups on the biochar's surface played an important role in activating persulfate, which could greatly enhance the degradation of pollutants [28]. Therefore, biochar can be used as an efficient adsorbent and an activator of persulfate to remove pharmaceutical pollutants.

Based on the above information, the following conclusions can be drawn: (1) Drug residues are widely found in surface water and groundwater, posing a serious threat to human health and ecological balance. (2) Adsorption and persulfate-based AOPs are effective and promising removal strategies. (3) The use of biochar for adsorbents and persulfate activators is cheap and highly efficient. As shown in Figure 2, many studies have been carried out regarding the removal of pharmaceutical pollutants. But there is still a lack of detailed summaries on the mechanisms of removing pharmaceutical pollutants

using both the adsorption and activation of persulfate using biochar. Therefore, this paper focuses on the mechanism of two removal paths, namely, the adsorption mechanism of the adsorption pathway and the main attack sites of free and non-free radicals towards various pharmaceutical pollutants in persulfate-based AOPs. In addition, the effects of pH, coexisting ions, the solution temperature, the biochar dosage, and the persulfate dosage on the removal of pharmaceutical pollutants are also concluded. This review helps researchers to systematically treat pharmaceutical pollution and also provides a rational support framework for the removal of other pharmaceutical pollutants in the future.

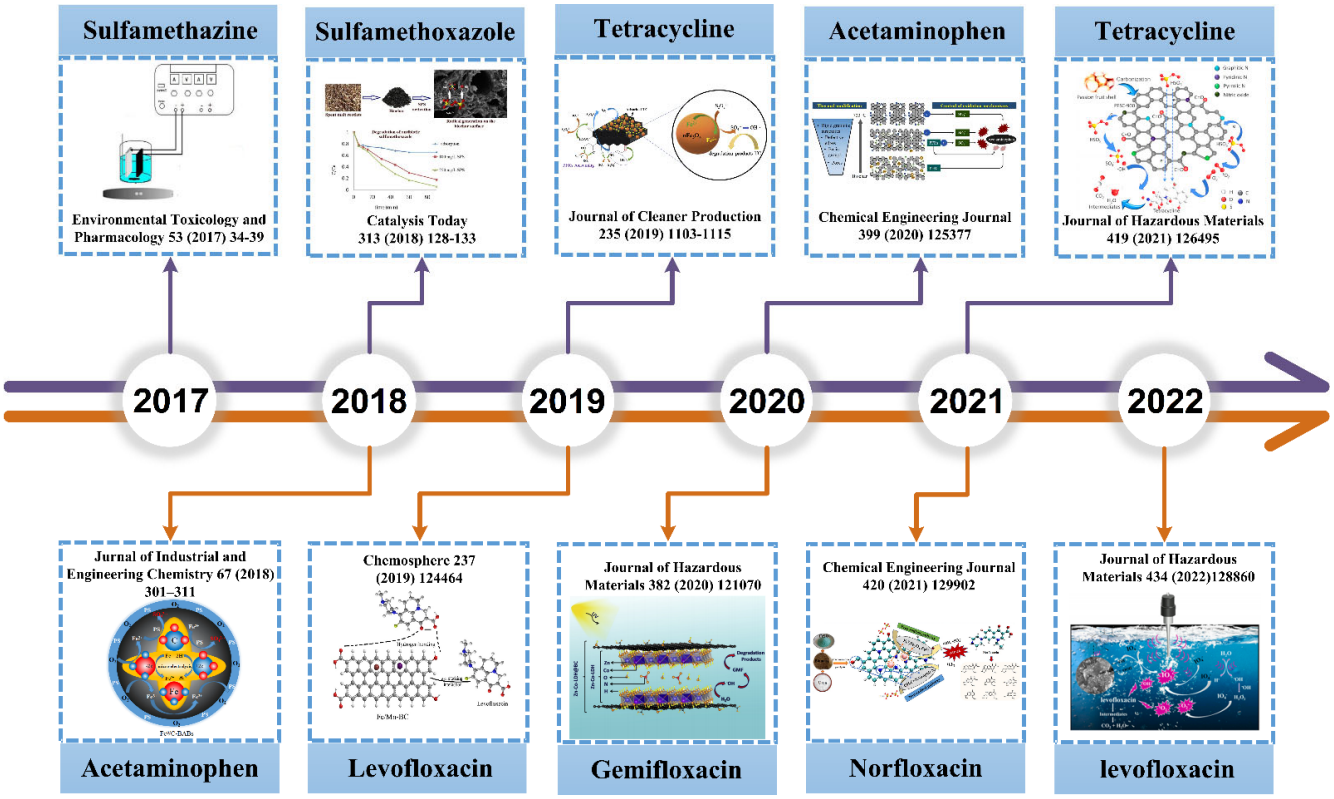

Figure 2. Timeline of outstanding works with respect to removing pharmaceutical pollutants [29–38].

2. Removal Mechanism

As shown in Figure 3, the removal of pharmaceutical pollutants by biochar mainly includes an adsorption pathway and a degradation pathway via persulfate-based AOPs. Each path has practical value for the removal of pharmaceutical pollutants.

2.1. Adsorption

Due to the porous structure of biochar's surface, biochar can be used for the adsorption and removal of pharmaceutical pollutants. It has the advantages of convenient operation and a simple structure design [39], and it has more economic benefits than reverse osmosis, ion exchange, and electrolysis [40]. The adsorption process usually includes three stages: external diffusion, particle diffusion, and surface reaction [41]. Adsorption mechanisms based on biochar include physical and chemical interactions [42]. In general, physical adsorption is mainly caused by the polarity of adsorbate molecules and the adsorbent surface, including processes such as pore filling, surface complexation, electrostatic attraction, hydrophobic interaction, π–π interaction, etc. [43]. It is a non-specific process guided by relatively weak attractive forces. Chemisorption is specific and can be achieved by sharing electron pairs to form chemical bonds between the adsorbent and the adsorbate [44]. Most of the adsorption removal of pharmaceutical pollutants is not limited to either physical

adsorption or chemical adsorption; they can occur simultaneously and complement each other [45].

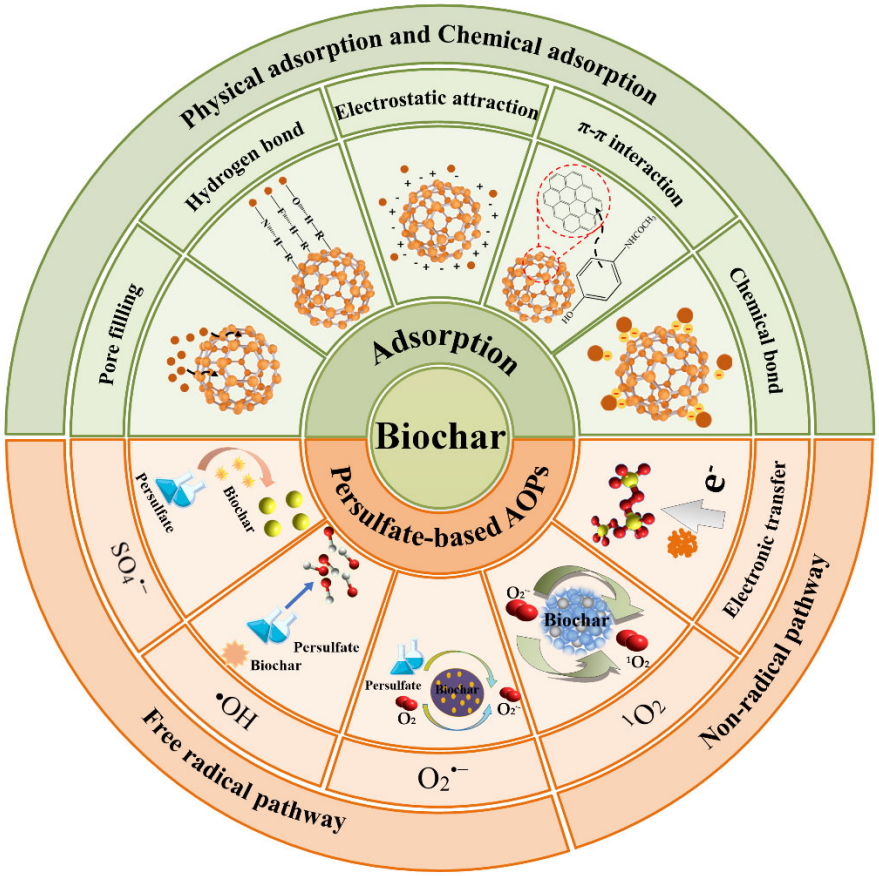

Figure 3. Removal mechanisms and main interactions of pharmaceutical pollutants by biochar.

2.2. Degradation via Persulfate-Based AOPs

AOPs provide a means to degrade pharmaceutical pollutants by inducing the production of reactive oxygen species (ROS) [46]. In general, there are many advanced oxidation processes, including ozone oxidation, Fenton oxidation, persulfate oxidation, etc. Among them, persulfate-AOPs have better pH adaptability and selective oxidation, and have become an efficient strategy for degrading pharmaceutical pollutants [47]. The degradation of pharmaceutical pollutants by persulfate-based AOPs mainly includes a free radical pathway and a nonradical pathway. The nonradical pathway can be divided into electron transfer and the application of singlet oxygen ($^1O_2$).

2.2.1. Free Radical Pathway

During the degradation process of pharmaceutical pollutants, free radical pathways are extremely important [48]. Generally, there are three kinds of free radicals involved in the degradation system of persulfate-based AOPs: $SO_4^{\bullet-}$, •OH, and $O_2^{\bullet-}$ [49]. During the degradation process, the main active species are also different due to the different pollutants and biochar. As a strong oxidant, $SO_4^{\bullet-}$ has a standard redox potential of 2.5–3.1 V, which can rapidly oxidize many kinds of organic pollutants and has high selectivity. In addition, the existence time of $SO_4^{\bullet-}$ is relatively long and $SO_4^{\bullet-}$ can exist in a wide pH range (2–9), which is conducive to a full reaction with pharmaceutical pollutants. Active sites on biochar's surface can catalyze persulfate to generate $SO_4^{\bullet-}$ (Equations (1)–(3)). The advanced oxidation process using •OH is a recognized clean and safe technology, and •OH also has a relatively strong oxidation effect. Pollutants and their intermediates can be easily decomposed into H_2O and CO_2 in an instant [50]. •OH can be produced by the

reaction of $SO_4^{\bullet -}$ and OH^- (Equation (4)). $O_2^{\bullet -}$ has a relatively weak oxidation capacity and a limited reactivity with organic pollutants, so its main role may be to participate in the catalytic process as an intermediate [51]. $O_2^{\bullet -}$ can be produced by dissolved oxygen (Equation (5)). Free radicals have three very significant characteristics: a strong reactivity, paramagnetic qualities, and a short lifespan [52]. In the process of molecular bonding, the unpaired electrons of free radicals have a strong tendency to pair. Therefore, most free radicals are relatively active, highly reactive, and easily react to form stable molecules. However, the existence time of free radicals is short, and the half-life of $SO_4^{\bullet -}$, which has a relatively long lifetime, is only 30–40 μs.

$$\text{Biochar's surface} - OH + S_2O_8^{2-} \rightarrow \text{Biochar's surface} - O^{\bullet} + SO_4^{\bullet -} + HSO_4^- \quad (1)$$

$$\text{Biochar's surface} - OOH + S_2O_8^{2-} \rightarrow \text{Biochar's surface} - OO^{\bullet} + SO_4^{\bullet -} + HSO_4^- \quad (2)$$

$$\text{Biochar's surface} - O + S_2O_8^{2-} \rightarrow \text{Biochar's surface} - O^{\bullet} + 2\,SO_4^{\bullet -} \quad (3)$$

$$SO_4^{\bullet -} + OH^- \rightarrow {\bullet}OH + SO_4^{2-} \quad (4)$$

$$O_2 + e^- \rightarrow O_2^{\bullet -} \quad (5)$$

2.2.2. Non-Radical Pathway

Non-radical pathways also exist in persulfate-based AOPs, including singlet oxygen ($^1O_2$) and electron transfer. The non-radical pathway can play a role in a wide range of pH conditions, including basic, neutral, and acidic conditions. In addition, non-radical pathways can reduce interference from inorganic or organic compounds. Moreover, the oxidative power of persulfate can be fully exploited in a non-radical pathway.

In the electron transfer process, the pharmaceutical pollutants are the electron donor, the biochar is the electron conductor, and the persulfate is the electron acceptor [53,54]. Electrons are transferred from the adsorbed pharmaceutical pollutants to the oxidant through the surface of biochar, which prevents the rapid recombination of electron and hole pairs, thereby increasing the degradation efficiency. The rate of electron transfer is closely related to the degree of graphitization and porosity of biochar [55]. The modification of biochar can reduce the surface resistivity and improve the efficiency of electron transfer. Biochar activated by HNO_3, $ZnCl_2$, and KOH has a broad spectrum of functional groups, a high specific surface area, a more abundant pore structure, etc., which are beneficial for improving its electron transfer ability [56–58]. Heteroatom doping can also increase electron transfer rates. Ye et al. [59] found that the incorporation of nitrogen with a high electronegativity and unpaired electrons could increase electron density and facilitate π electron flow.

$^1O_2$ is highly selective as an oxidant since it has an unoccupied π_{2p} molecular orbital, and thus possesses strong electrophilic reactivity. On the one hand, $^1O_2$ can be generated by the self-degradation of persulfate (Equations (6)–(8)). On the other hand, carbonyl/ketone groups can be considered as active sites for the generation of $^1O_2$. $^1O_2$ can react with most of the unsaturated pharmaceutical pollutants through electrophilic addition. In a recent study, $^1O_2$ exhibited a strong oxidative power for electron-rich organic compounds under weakly acidic conditions (pH ≥ 5) during advanced oxidation processes [60]. It can attack the -NH_2 group aligned to the benzene ring to form dimer products that could be adsorbed on the biochar's surface to efficiently remove pollutants [61]. It can also attack the sulfonamide group to achieve the efficient degradation of sulfonamide drugs [62]. But for most pharmaceutical pollutants, the kinetic rate of $^1O_2$ is lower than that of free radicals. Therefore, various strategies and key methods should be adopted for the rational application of $^1O_2$ to maximize the degradation efficiency.

$$S_2O_8^{2-} \rightarrow 2SO_4^{\bullet -} \quad (6)$$

$$SO_4^{\bullet -} + H_2O \rightarrow {\bullet}OH + HSO_4^- \quad (7)$$

$$4\bullet OH \rightarrow {}^1O_2 + 2H_2O \quad (8)$$

3. Adsorption and Degradation Behaviors of Various Drugs

Taking TC, SMX, ACT, CPX, and LEV as examples and supplementing them with other pharmaceutical pollutants, their removal behaviors were studied through adsorption and degradation via persulfate-based AOPs, respectively. All five major pollutants can be detected by high performance liquid chromatography-tandem mass spectrometry. Table 1 summarizes the basic properties and applications of TC, SMX, ACT, CPX, and LEV.

Table 1. Basic properties and applications of TC, SMX, ACT, CPX, and LEV.

Target Pollutants	Formula	Molecular Weight (g/mol)	Molar Volume	Solubility (mg/mL)	Application	Ref.
TC	$C_{22}H_{24}N_2O_8$	444.43	270.3 m^3/mol	1.7	For rickettsial disease, mycoplasma infection, chlamydia infection, etc., caused by sensitive microorganisms	[36]
SMX	$C_{10}H_{11}N_3O_3S$	253.28	173.1 cm^3/mol	Almost insoluble in water	For respiratory system infection, intestinal infection, and wound infection caused by sensitive bacteria, etc.	[18]
ACT	$C_8H_9NO_2$	151.16	120.9 cm^3/mol	14	Used to relieve both fever and pain of various causes	[63]
CPX	$C_{16}H_{17}N_3O_4S{\cdot}H_2O$	365.4	231.3 m^3/mol	13.5	Used to treat multiple site infections caused by sensitive bacteria	[64]
LEV	$C_{18}H_{20}FN_3O_4$	361.37	243.9 cm^3/mol	50	For the treatment of respiratory tract infections caused by bacteria, mycoplasma, etc.	[65]

3.1. Tetracycline

3.1.1. Adsorption

TC can be removed by means of adsorption. The adsorption of TC can be divided into two stages. The first stage is the fast adsorption stage, which can adsorb and remove a large amount of TC in a short time [66]. Since the adsorbent can generate many micropores, TC can diffuse into the adsorbent through most of the adsorption sites exposed on the adsorbent surface [67]. The aromatic ring structure of TC molecules can bind tightly with π electrons in biochar, acting as π electron acceptors and accelerating the occurrence of π–π interactions. There are a large number of polar groups on TC molecules, such as -OH and -NH_2 [68], and there are 8 H-bond donors and 11 H-bond acceptors in each TC molecule [69]. The C-H groups of biochar can form hydrogen bonds with functional groups such as phenolic hydroxyl groups on the surface of TC to adsorb TC [70]. In the second stage, the adsorption gradually slows down and eventually reaches equilibrium, at which point the biochar has reached saturation. [71].

3.1.2. Degradation via Persulfate-Based AOPs

The use of persulfate-based AOPs has been shown to be an efficient method for TC removal, which can be realized by external energy excitation and heterogeneous catalytic processes [72]. During the degradation process, TC was first degraded into intermediates, which were further cracked into small molecules, and finally completely oxidized into carbon dioxide and water molecules. Figure 4a shows the effects of three quenching agents—EtOH, TBA, and FFA—on TC degradation [73]. It was observed that the addition of EtOH and TBA had little effect on the degradation of TC, indicating that the contribution of $SO_4^{\bullet-}$ and •OH was small, while with the increase of the FFA addition, the degradation efficiency of TC decreased rapidly, indicating that $^1O_2$ contributed more in the non-radical pathway. As shown in Figure 4b, the active species were captured using TEMP as traps. It

was further proved that $^1O_2$ played an important role in the degradation of TC [73]. The two degradation pathways of TC are depicted in Figure 4c [36]. In pathway I, the C-N bond in TC was cleaved and demethylated to yield P1 and P2. The dehydration of P2 yielded P3 and P6. P3 was further converted to P4 and P5 by ring cleavage. The second pathway involved C–C, C–N, and C=C bonds being attacked by reactive oxygen species (including $SO_4^{\bullet-}$, •OH, and $^1O_2$) and transferred electrons, resulting in hydroxylation, demethylation, cleavage, and decarboxylation [74]. The formation of P7, P8, and P9 were caused by the successive hydroxylation of the rings by $^1O_2$ attacking the $–NH_2$ group on the benzene ring, leading to its demethylation, while the formation of P10 was caused by the $–CH_3$ and $–NH_2$ demethylation of P9. Oxidation-induced ring cleavage yielded the ring-opening products P11 and P12. These intermediates were further oxidized to generate CO_2, H_2O, and other inorganic ions. Briefly, TC was degraded through dehydration, the loss of dimethylamino groups, the cleavage of amino rings, and double bond and aromatic epoxidation.

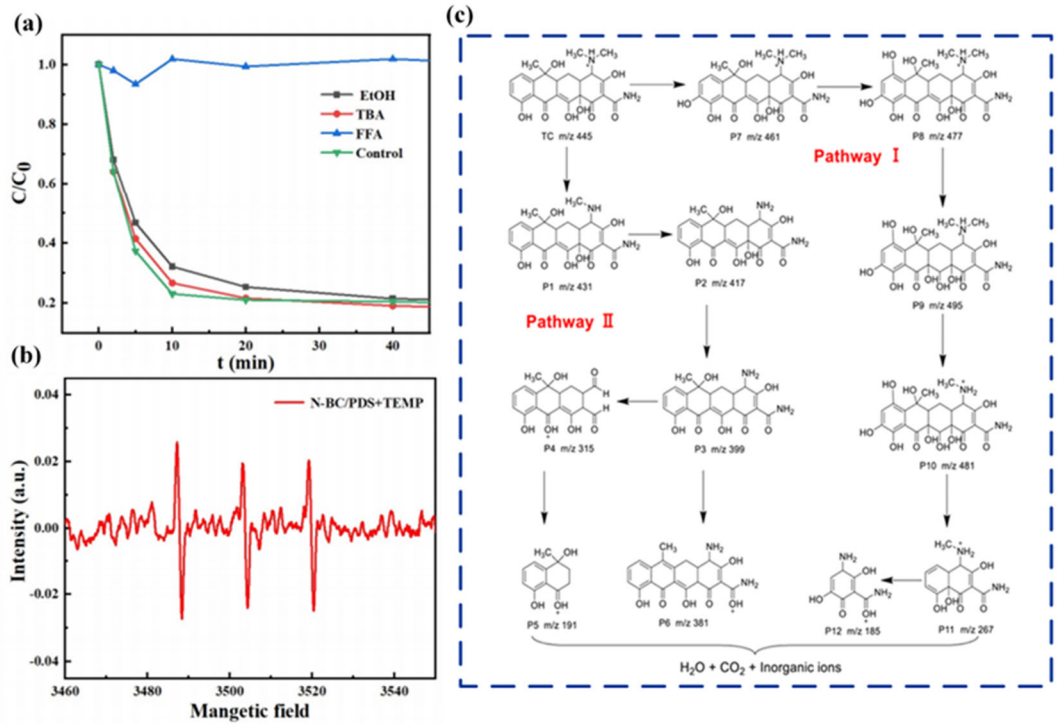

Figure 4. Effects of three quenchers on TC degradation (**a**) [73]; TEMP-$^1O_2$ at different reaction times (**b**) [73]; Degradation pathway of TC (**c**) [36].

3.2. Sulfamethoxazole

3.2.1. Adsorption

The removal of SMX by biochar can be achieved by adsorption. Many adsorption experiments have shown that SMX and biochar can form various adsorption mechanisms through π–π electron donor-acceptor, hydrogen-bond, and hydrophobic interactions. SMX is composed of an aromatic benzene ring and an aromatic heterocyclic group, which can interact with the aromatic ring on the surface of the highly carbonized biochar through π–π electron coupling, thereby achieving the effect of adsorption [75]. Another important mechanism is the formation of hydrogen bonds between dissociated H and electron-friendly atoms such as N, O, and F [76,77]. Through theoretical calculation, it was found that many nitrogen and oxygen atoms in SMX are electronegative and can form hydrogen bonds with the dissociated H on the surface of biochar. Hydrophobic interactions number among the pH-dependent adsorption mechanisms for SMX adsorption by biochar [78]. SMX is more difficult to dissolve at a high pH than at a low pH, which makes its adsorption capacity on the surface of hydrophobic biochar higher [79]. Therefore, the partial adsorption of

SMX on biochar can be attributed to the hydrophobic interaction between SMX and the hydrophobic surface of biochar.

3.2.2. Degradation via Persulfate-Based AOPs

SMX can be degraded by persulfate-based AOPs. The catalytic degradation of SMX involves free-radical and non-radical pathways. As shown in Figure 5a–f, $SO_4^{\bullet-}$, •OH, $^1O_2$, and $O_2^{\bullet-}$ all participated in the degradation of SMX, of which $^1O_2$ and $O_2^{\bullet-}$ contributed the most [80]. Density functional theory calculations have proved that the S-N bonds near the S atoms in SMX are sensitive sites for radical attack [18]. As a selective oxidizing species, $^1O_2$ exhibits ahigh reactivity towards electron-rich groups of SMX molecules. The sulfonamide group in the SMX molecule is more vulnerable to $^1O_2$ attack, while the isoxazole ring in the SMX molecule is not a sensitive site for $^1O_2$ attack [81]. The biochar with a lower degree of graphitization could obtain the final product after only one hydroxylation reaction, while the biochar with a higher degree of graphitization required multiple degradation steps. The specific degradation pathway is shown in the Figure 5g. First, the parent SMX was converted to product A by hydroxylation [82]. It was subsequently converted to product B through dehydroxylation and oxidation processes. Due to the interaction of $SO_4^{\bullet-}$ and •OH, the S-N bond was easily broken [83,84], and then product C was obtained. Finally, product D was obtained due to deamination and dehydroxylation.

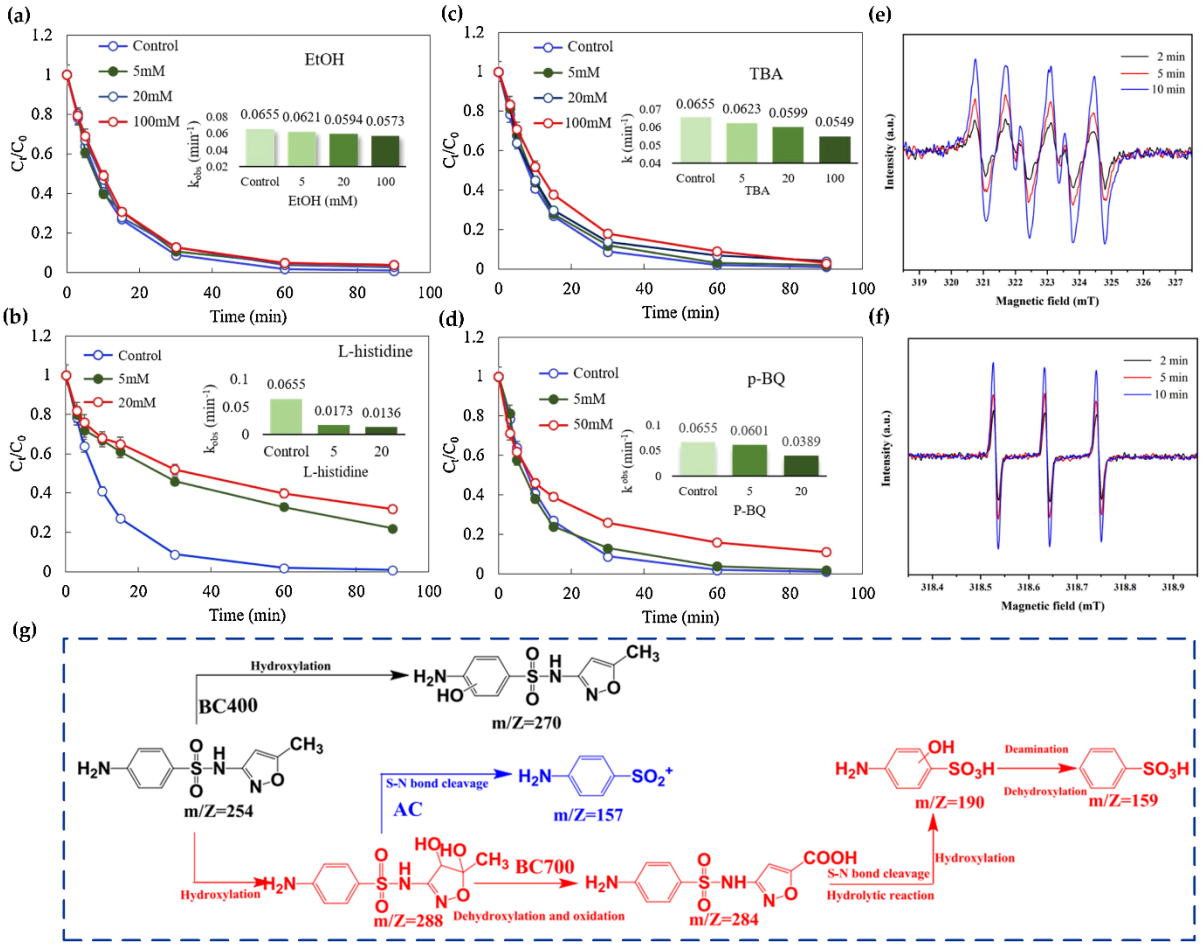

Figure 5. Quenching tests using different scavengers (**a**) EtOH; (**b**) L-histidine; (**c**) TBA; (**d**) p-BQ [81]; EPR spectra using DMPO for (**e**) $O_2^{\bullet-}$ and TEMP for (**f**) $^1O_2$ [80]; (**g**) Intermediates and degradation pathways [18].

3.3. Acetaminophen

3.3.1. Adsorption

The key mechanisms for ACT removal by adsorption are π–π interactions, hydrogen bonding, and electrostatic interactions. The π–electron interaction is a key mechanism for the adsorption of aromatic compounds. The phenolic hydroxyl and amide group in the ACT are powerful electron donors that can trigger the aromatic ring to obtain a large number of electrons and interact with delocalized adsorbed electrons. ACT molecules can exhibit nitrogen-resonance electron pairs in acidic media [10]. Therefore, ACT can act as a π-donor. Electrostatic interactions occur when ionized molecules of ACT are transferred to the charged adsorbent surface. However, this interaction is lower when the adsorbent is zwitterionic or when the surface net charge is zero. Electrostatic repulsion occurs when the adsorbent surface and the adsorbate have the same charge [85]. Previous studies have shown that proton acceptor groups (such as –OH and –C=O) in ACT molecules and N with strong electronegativity can have strong hydrogen-bonding interactions with biochar [86].

3.3.2. Degradation via Persulfate-Based AOPs

ACT can be degraded by free-radical and non-radical pathways, among which the radical pathway dominated by $SO_4^{\bullet-}$ and •OH plays an important role. According to previous studies, the acetyl amino group of ACT was easily attacked by $SO_4^{\bullet-}$ [87], and •OH mainly attacked the substituents on the benzene ring of ACT, and then formed hydroquinone or 4-benzoquinone to help benzene ring-opening [88]. $O_2^{\bullet-}$ and $^1O_2$ contributed to ring-opening and hydrogen abstraction reaction [89]. The specific degradation process and pathway are shown in Figure 6a,b. ACT first underwent hydroxylation reaction to form P1. In pathway I, P1 was further reacted with •OH to produce P2 and was then oxidized to P3. In pathway II, since the acetyl amino group of ACT was easily attacked by $SO_4^{\bullet-}$, P1 was oxidized to P4, and P5 was generated through an attack of a hydroxyl radical on aromatic ring. There were three pathways after P5. In pathway II-1, P5 generated P6 through hydrogen abstraction dominated by $O_2^{\bullet-}$ and $^1O_2$, and then P3 and P7 were obtained due to a ring-opening reaction [90]. In addition, P5 could be directly mineralized to the low-molecular compound P10 via a ring-opening reaction or transformed into P8 via hydroxylation and then P8 opened the ring to the P9 [91]. In pathway III, acylamide and phenol hydroxy on P5 were attacked through the combined action of $SO_4^{\bullet-}$ and •OH to form P11 and were further oxidized to small molecular compounds. In pathway IV, P1 was transformed into P12 via a ring-open reaction and further degraded to P13.

(a)

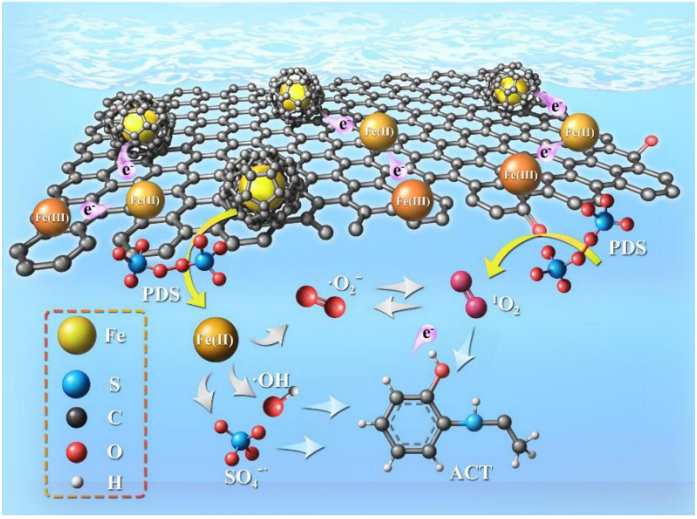

Figure 6. *Cont.*

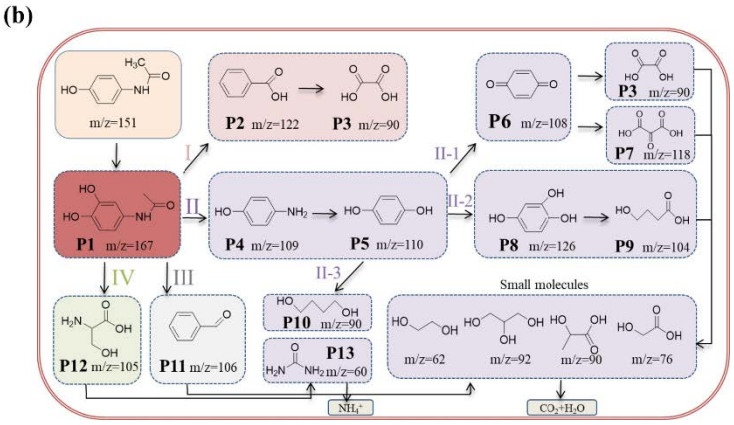

Figure 6. The degradation process of ACT (**a**) [92] and the proposed degradation pathaway of ACT (**b**) [92].

3.4. Cephalexin

3.4.1. Adsorption

The adsorption mechanism of biochar to CPX is mainly hydrogen bond interactions, electrostatic interactions, and hydrophobic interactions [93]. Biochar contains abundant oxygen-containing functional groups, such as C=O, –COOH, –OH, etc., which can form hydrogen bonds with the N-H functional groups of CPX [94]. π electrons in biochar, due to electrostatic action, can combine with the aromatic ring part of the TC molecule, which promotes π–π interaction, thus enhancing adsorption [93]. When there are fewer oxygen-containing functional groups on the surface of biochar, the surface is more hydrophobic, which in turn will generate hydrophobic interactions with CPX to promote adsorption [95,96].

3.4.2. Degradation via Persulfate-Based AOPs

The degradation mechanism of CPX is shown in Figure 7a. •OH and $SO_4^{\bullet-}$ were the main free radicals for the degradation of CPX [64]. The degradation pathway of CPX is shown in Figure 7b. During the degradation process, P1 was first formed by the cleavage of the β-lactam ring and the addition of a hydroxyl to replace the methyl group in the CPX molecule [94], followed by the cleavage of the C–N bond at the marker of the carboxyl loss, which divided the intermediate into two groups (A and B). The A1 universal hydroxyl group replaced the amide group to form A2 and further oxidized to A3. Subsequently, A4 was obtained due to the deamination of A2, and then A5 was produced via the deamination of A4. Acetic acid and benzene were generated resulting from the further cleavage of A5 and A3 [97]. For group B, B2 was derived from the hydroxylation of B1. In addition, B3 and B4 were formed by dehydration, while H_2O and O atoms were lost, respectively. On the other hand, B5 was produced via the loss of amidogen of B1. B6 and B7 were further formed due to the loss of hydroxyl and oxygen atoms [98]. Finally, these intermediates were further decomposed into CO_2, H_2O, and small molecular components.

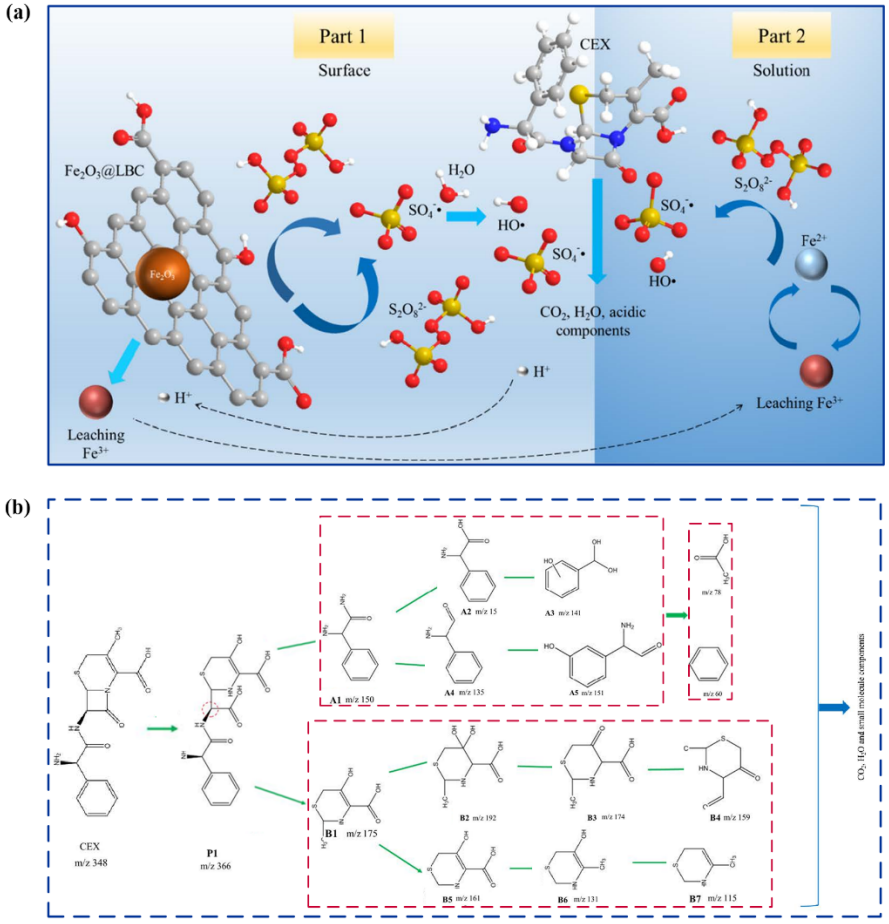

Figure 7. Possible mechanism of persulfate activation by biochar for CPX degradation (**a**) [64]; Proposed reaction pathway for the degradation of CPX (**b**) [64].

3.5. Levofloxacin

3.5.1. Adsorption

The mechanism of biochar's adsorption of LEV can be attributed to electrostatic interactions, H-bonding, functional groups' complexation, π–π stacking interaction, and π–π electron donor–acceptor interactions [99]. The adsorption process of LEV onto biochar was dominated by monolayer-homogeneous and chemical adsorption [100]. The maximum adsorption of LEV by biochar occurred in neutral and weakly acidic environments, which may be due to the fact that most LEV exist in the form of LEV^0 at pH = 6–7, and the decrease in the molecular distance caused by the weak electrostatic repulsion may promote the formation of π–π stacking between biochar and LEV [101]. In addition, the adsorption capacities of biochar were obviously increased at higher temperatures (25–45 °C) [100]. A thermodynamic analysis showed that the adsorption process was spontaneous and endothermic [102]. The adsorption effectivity increased by increasing the site energy of biochar's surface via a site energy distribution analysis. Abundant functional groups (e.g., –OH, –COOH, etc.) on the biochar's surface can increase the average site energy and site energy heterogeneity, thereby enhancing the adsorption of LEV [100].

3.5.2. Degradation via Persulfate-Based AOPs

The non-radical pathway dominated by $^1O_2$ and electron transfer played an important role in the degradation of LEV, and $SO_4^{\bullet -}$ in the radical pathway also contributed to the degradation of LEV (Figure 8a,b). During the degradation process, the vulnerable sites of LEV included the side with the piperazinyl and quinolone moieties and the benzene ring [65]. In order to further explore the degradation pathway of LEV, the intermediate

products were detected by LC-MS (Figure 8c). The degradation of LEV included the mechanisms of demethylation, depiperazinylation, and carboxylation/decarboxylation [103]. In pathway I, P14 was formed from the piperazinyl dealkylation of LEV by electrophilic and free radical reactions [104]. P11 could also be produced from the piperazinyl oxidation and opening of LVF via attacking through radicals or electrophilic reactions [105]. P13 was obtained due to decarboxylation of P14. P9 was generated resulting from the oxidation and decarboxylation acid of the piperazine ring of P13. P9 was also produced via the oxidation and carboxylation of P11 [104]. In Pathway II, P16 was obtained due to the replacement of the F^- group by the hydroxyl group. P12 formed under radical attack via two pathways: (1) the decarboxylation process of P16 and (2) the cleavage of the piperazine chain P16. P10 could be generated via the oxidation of the piperazine ring and decarboxylation and hydroxyl addition of P16 mainly under the continuous effect of the $SO_4^{\bullet -}$ and $^1O_2$. P8 could be produced via the cleavage of N-C bond on P12. P6, P4, P2, and P1 could be gradually formed mainly under the attack of $SO_4^{\bullet -}$ and $^1O_2$ via the oxidation and destruction of the quinolone moiety [106].

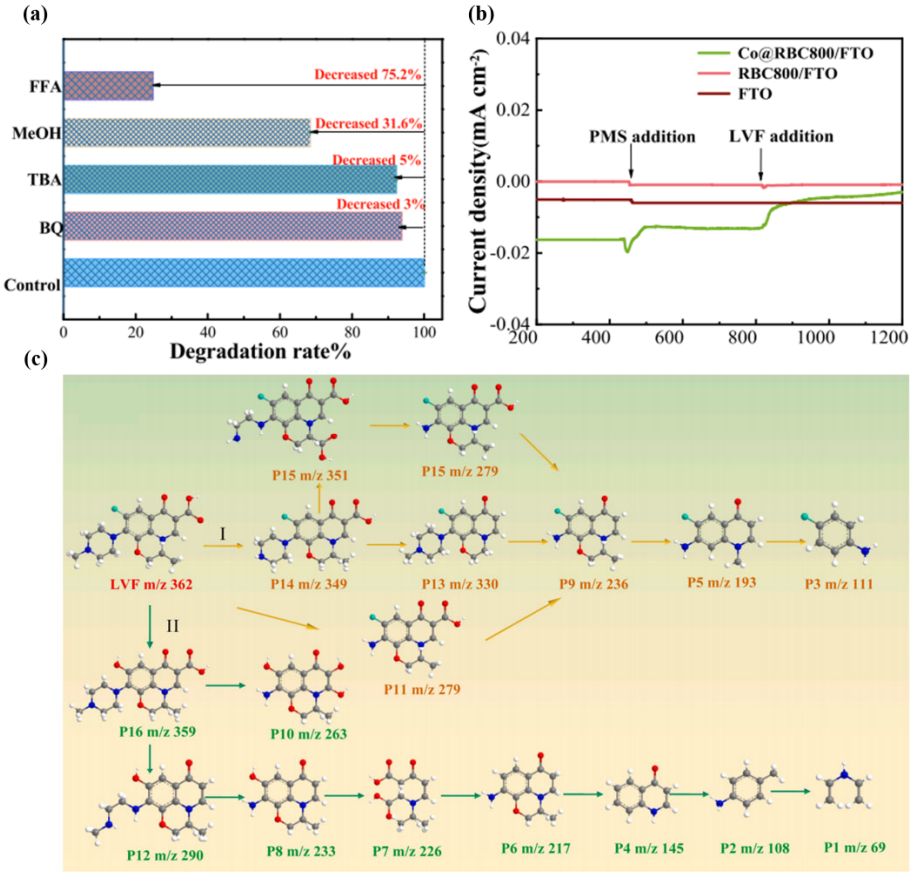

Figure 8. Quenching effect on LEV degradation by different scavengers (**a**) [65]; i–t curves with peroxymonosulfate and LEV addition (**b**) [65]; Possible degradation pathway of LEV (**c**) [65].

3.6. Other Drugs

In addition to the abovementioned main pharmaceutical pollutants, the pollution caused by other pharmaceutical pollutants is also becoming more and more common. Tables 2 and 3 summarize their removal procedures using biochar from the degradation via persulfate-based AOPs and adsorption, respectively.

Table 2. The removal of other pharmaceutical pollutants by biochar through degradation via persulfate-based AOPs.

Target Pollutants	Catalyst	Catalyst Dosage (g/L)	Pollutant Concentration (mg/L)	Persulfate Dosage (mM)	pH	Reaction Temperature (°C)	Reaction Time (min)	Vulnerable Areas	Degradation Efficiency. (%)	Ref.
Metronidazole (MNZ)	Potassium-doped magnetic biochar (KMBC)	0.5	20.0	1.0	6.5	25	180	C–N, $–NO_2$	98.40	[107]
Norfloxacin (NOR)	Iron and nitrogen co-doped biochar material (Fe@N co-doped biochar)	0.1	10.0	10	7	25	20	the nalidixic and piperazine rings	95	[108]
Sulfadiazine (SDZ)	Biochar-based iron material (MBC)	1.0	40.0	1.5	5.16	25	60	N–H, S–N, C–S	91.97	[109]
Phenol	Demineralized biochar (DSS700)	0.5	200.0	10	7	25	800	benzene-OH	57.80	[110]
Arbidol (ARB)	Biochar-supported red mud (RM-BC)	0.2	20	0.6	7	25	15	Sulfur atom, 4-(dimethylamino) methyle group	100	[111]
Gemifloxacin (GMF)	Biochar nanocomposite (Zn-Co-LDH)	0.75	15	20	5.5	35	130	C=C, –OH, C–O, C–N	92.7	[38]
P-hydroxybenzoic acid (HBA)	Biomass-derived N-doped porous carbon (Y-PC)	0.05	20	5.7	4.5	25	120	–OH	97.6	[112]

Table 3. The removal of other pharmaceutical pollutants by biochar through adsorption.

Target Pollutants	Adsorbent	Adsorbent Dosage (g/L)	Pollutant Concentration (mg/L)	pH	Time	Isotherms/Kinetics	Adsorption Capacity (mg/g)	Mechanism	Ref.
Ibuprofen (IBP)	Biochar from pepper stems (PS-biochar)	1.0	40	7	240 min	Langmuir/ Pseudo-second-order	596.6	π–π interaction, pore filling, H-bonding	[113]
Ciprofloxacin	Ga_2S_3 and sulfur co-modified biochar (Ga/S-BC)	0.25	140	5	60 min	Langmuir/ Pseudo-second-order	330.21	Electrostatic interaction, hydrogen bonding, π–π interactions.	[114]
Sulfadiazine	Tea waste biochar	0.5	50	10.97	720 min	Langmuir/ Pseudo-second-order	99.47	π–π interactions.	[115]
Naproxen	Peanutshells-derivedbiochars	5.0	1000	7	1440 min	Langmuir/ Pseudo-second-order	81.6	π–π interactions.	[116]
Fluoxetine	Biochar	2.3	50	7.1	60 min	Freundlich/Pseudo-second-order	70	Electrostatic attractions	[117]
Antibiotic fermentation residues (AFRB)	Sludge (AFSB)	0.01	40	7	12 h	Pseudo-first-order	82.6	Aromatic structures, the chemisorption, active sites	[118]
Amoxicillin antibiotic (AMX).	Giant reed (AMX)	0.5	250	7	400 min	Sips isotherm/ Pseudo-second-order	345.4	Hydrogen bonding, aromatic structures, the chemisorption, active sites	[119]

4. Effect of Parameters

4.1. Effect of Solution pH

The solution pH affects reactive oxygen species, the surface charge of biochar, and the dissociated form of the target antibiotic. First, the generation of active species in the free radical and non-radical pathways is pH-dependent. In a free radical pathway, under acidic conditions, the dominant species is $SO_4^{\bullet -}$, and under alkaline conditions, the dominant species is •OH radicals. Since under alkaline conditions the solution contains more hydroxide ions, $SO_4^{\bullet -}$ can react with water or a hydroxyl to generate •OH [120]. In the non-radical pathway, $^1O_2$ exhibits a strong oxidative ability for electron-rich organic compounds under weakly acidic conditions (pH $\geq$ 5) and can rapidly degrade pollutants [60]. Second, when the solution pH is lower than the zero potential of the carbon material, the carbon's surface has strong affinity for anionic pollutants [121]. Finally, the solution pH is closely related to the dissociated form and degree of deprotonation of the antibiotic. For instance, TC can exist in three forms depending on the pH: it is cationic at pH < 3.3, dipolar (zwitterionic) at 3.3 < pH < 7.7, and negatively charged at pH < 7.7 [122]. Furthermore, it should be noted that increased doses of persulfate can also lead to a decrease in pH and an increase in inorganic ions, which will reduce the efficiency of biochar with respect to cleansing water bodies [123].

The effect of the solution pH on the adsorption path to remove pharmaceutical pollutants is due to electrostatic interactions, ion exchange, π–π EDA interactions, and so on [122]. Sun et al. [124] found that the main mechanism of pH value on the adsorption removal of SMX was based on the protonation/deprotonation of SMX at different pH values. At pH < 1.7, 1.7 < pH < 5.6, and pH > 5.6, SMX presented cationic, neutral, and anionic states, respectively. When the 4 < pH < 6, the adsorption capacity for SMX was the strongest. The H-bond is the main mechanism at pH = 6, while the ion–dipole/charge-dipole force may be the key role at pH = 4–5. Furthermore, SMX absorption depends on π–π interactions.

4.2. Effect of Coexisting Ions

The degree of the adsorption of pharmaceutical pollutants by different biochar types can be attributed to space limitations [125], electrostatic interactions [126], and the properties of biochar functional groups [127]. Different ions have different effects on the removal of pharmaceutical pollutants by biochar adsorption. Anions have little effect on biochar adsorption, while cations can promote and inhibit adsorption to varying degrees [93]. Pan et al. [128] reported that when Na^+ and Ca^{2+} existed in the solution, the surface functional groups would react with these ions to reduce the adsorption of TC by biochar. At the same time, these ions also occupied the adsorption position. The same results were reported by Hammond et al. [129] On the contrary, the presence of some ions sometimes promotes the adsorption of pollutants. Xiang et al. [29] reported that the presence of Na^+ led to an increase in the adsorption capacity of LEV. This tendency may be because the salting out of pharmaceutical pollutants reduces their solubility in water, thereby enhancing the adsorption of biochar.

Persulfate-based AOPs are also affected by different ions (Cl^-, CO_3^{2-}, HCO_3^-, NO_3^-, NO_2^-, HPO_4^{2-}, and $H_2PO_4^-$). This is mainly because these ions have a scavenging effect on different free radicals. In general, NO_3^-/NO_2^- and $HPO_4^{2-}/H_2PO_4^-$ have little effect under certain concentrations. Liu et al. [130] reported that although NO_3^-/NO_2^- and $HPO_4^{2-}/H_2PO_4^-$ would block the catalytically active sites on carbon-based materials, resulting in reduced catalytic activity, their reactions with •OH and $SO_4^{\bullet -}$ were too slow to be ineffective at ordinary concentrations. Therefore, the effects of NO_3^-/NO_2^- and $HPO_4^{2-}/H_2PO_4^-$ on the catalytic process are insignificant. Yang et al. [131] reported that PO_4^{3-} may also promote peroxymonosulfate's activation under certain conditions. According to previous research, Cl^- exhibited a significant inhibitory effect at low concentrations. Cl^- above a certain concentration value will promote the removal of organic pollutants. Since it was discovered that $SO_4^{\bullet -}$ and •OH can react with Cl^- to generate less

active Cl•, the presence of Cl^- might reduce the oxidation efficiency. On the contrary, at high concentrations, the generated Cl• was converted into active chlorine (Cl_2 and HClO), which improved the catalytic performance [132]. The effects of CO_3^{2-} and HCO_3^- on the degradation were completely opposite to that of Cl^-, and low concentrations of CO_3^{2-} and HCO_3^- could enhance the catalytic degradation process. However, high concentrations of CO_3^{2-} and HCO_3^- inhibit the catalytic degradation process. Jiang et al. [133] and Liu et al. [134] found that the hydrolysis of CO_3^{2-} and HCO_3^- would lead to an increase in the solution pH at low concentrations. This results in the decomposition of HSO_5^- into SO_5^{2-} and the formation of $^1O_2$. At the same time, CO_3^{2-} and HCO_3^- can remove $SO_4^{\bullet-}$ and •OH to obtain $^1O_2$ indirectly. However, high concentrations of CO_3^{2-} and HCO_3^- have a strong inhibitory effect on the degradation of pharmaceutical pollutants, which may be be related to the quenching effect of ions. Previous studies have also reported that CO_3^{2-} and HCO_3^- can quench $O_2^{\bullet-}$, further suppressing the generation of $^1O_2$ and inducing a decrease in catalytic performance.

4.3. Effect of Solution Temperature

The reaction temperature is an important factor affecting the biochar-based removal of pharmaceutical pollutants. Choosing the appropriate temperature can greatly improve the degradation efficiency [135]. Generally speaking, an increase in temperature is conducive to overcoming the activation energy barrier and increasing the degradation rate of pharmaceutical pollutants. Simultaneously, due to the synergistic effect of the temperature rise and biochar, the system performance can also be significantly improved [136]. Raising the temperature can also promote the diffusion of pollutants and persulfates to the catalyst's surface, enhancing the contact between the pollutants, oxidants, and catalysts, which in turn degrades organic pollutants more efficiently in complex heterogeneous systems. Hu et al. [36], in an experiment involving the persulfate-activated persulfate degradation of TC in passion fruit biochar, demonstrated that as the temperature rose from 20 °C to 40 °C, the degradation rate of TC also increased from 82% to 93%. A higher temperature can activate persulfate to generate more active substances, promote the electron transfer process between the catalyst and persulfate, and is beneficial for the degradation of pharmaceutical pollutants. It is worth noting that despite the good degradation performance at high temperatures, the energy consumption should still be considered, and the reaction temperature should be reasonably controlled. For adsorption, since the reaction is endothermic, properly increasing the temperature is beneficial for the reaction to proceed [137].

4.4. Effects of Biochar Dosage

The effect of using solely persulfate to degrade pharmaceutical pollutants is extremely low, so persulfate activation with biochar is required. An increase in the catalyst dosage can provide more active sites for the activation of persulfate; then, more active species will be produced in the free radical and non-radical pathway, thereby improving the degradation rate. In addition, the increase in the dosage of biochar can also provide more adsorption sites to enhance the adsorption effect. Xiong et al. [138] used peroxodisulfate as a catalyst to degrade TC. When the dosage of the N-doped prolifera-derived magnetic biochar was increased from 0.1 g/L to 0.3 g/L, the removal rate of the pollutants had been greatly improved in the adsorption stage and catalytic stage. (The effect of adsorption was improved from 21% to 49%, and the catalytic degradation effect was improved from 75% to 88%).

4.5. Effects of Persulfate Dosage

The amount of oxidant directly affects the degradation performance of the biochar/persulfate system. In order to make the degradation rate reach the optimum value, it is necessary to select the appropriate amount of oxidant for the specific experimental situation. Regarding the biochar-activated persulfate degradation of phenolic compounds in water, Kleopatra Miserli et al. [139] mentioned that the persulfate concentration increased slightly,

and the degradation rate also increased. However, when the amount of persulfate was too high, the degradation rate did not change much. This phenomenon may be due to the limited amount of biochar relative to the persulfate concentration, which cannot provide enough active sites; therefore, the excess persulfate will consume the active species, converting $SO_4^{\bullet-}$ or •OH to $S_2O_8^{-}$ with poor oxidizing ability and oxygen (Equations (9)–(11)), resulting in a decrease in degradation performance [27]. Wang et al. [140] also demonstrated in the degradation of SMX by biochar/Fe^{3+} that the degradation rate of pharmaceutical pollutants was not always proportional to the amount of persulfate.

$$SO_4^{\bullet-} + S_2O_8^{2-} \rightarrow S_2O_8^{\bullet-} + SO_4^{2-} \quad (9)$$

$$HO\bullet + S_2O_8^{2-} \rightarrow S_2O_8^{\bullet-} + OH^{-} \quad (10)$$

$$3/2H_2O + S_2O_8^{\bullet-} \rightarrow 2SO_4^{2-} + 3/4O_2 + 3H^{+} \quad (11)$$

5. Conclusions and Future Prospects

5.1. Conclusions

This paper reviews the research progress on biochar in the field of treating pharmaceutical pollutants, including the removal path, the removal behavior, and the influence of operation parameters. The removal process of various pharmaceutical pollutants mainly includes the adsorption and degradation via persulfate-based AOPs. In the adsorption process, the removal methods of five kinds of pharmaceutical pollutants (TC, SMX, ACT, LEV, and CPX) are similar, mainly because the aromatic ring part of the drug is closely associated with the π electrons in the biochar, thereby accelerating the occurrence of π–π interaction to remove the pharmaceutical pollutants; then, the free hydrogen on the biochar's surface forms hydrogen bonds with the more electronegative functional groups on the surface of the drug molecule for further adsorption. The degradation via persulfate-based AOPs includes the free radical and the non-radical pathway. During the degradation process, the C-N bond on the TC molecule is attacked and cleaved, resulting in a demethylation effect. The S-N bonds near the S atoms in SMX are sensitive sites for radical attack and the sulfonamide group is more vulnerable to $^1O_2$ attack. The acetyl amino group of ACT is easily attacked by $SO_4^{\bullet-}$, and •OH mainly attacks the substituents on the benzene ring of ACT, and then forms hydroquinone or 4-benzoquinone to aid the opening of the benzene ring. For the degradation of CPX, $SO_4^{\bullet-}$ and •OH mainly attack β-the cleavage of the lactam ring and -OH of CPX. $SO_4^{\bullet-}$ and •OH attack the nitrogen atom of piperazine in LEV, leading to demethylation effects. Tables 4 and 5 summarize the removal conditions and reusability of five major pharmaceutical pollutants (TC, SMX, ACT, LEV, and CPX) in persulfate-based AOPs and adsorption, respectively. The pH value of the solution mainly affects the species of reactive oxygen species, the surface charge of carbon material, and the dissociation form of the target antibiotic. Coexisting anions affect the degradation efficiency of pharmaceutical pollutants in the free-radical pathway but have little effect on the non-free radical pathway.

Table 4. The removal of five major pollutants by biochar through degradation via persulfate-based AOPs.

Target Pollutants	Catalyst	Catalyst Dosage (g/L)	Pollutant Concentration (mg/L)	Persulfate Dosage (mM)	pH	Reaction Time (min)	Degradation Efficiency. (%)	Cycle Times	Last Efficiency (%)	Ref.
TC	biochart from tannery sludge (TSBC)	0.3	50	3	7	60	99.1	Four times	79.8	[141]
	nitrogen-doped biochar (N-BCX)	0.2	20	2	7	120	100	Three times	55	[142]
SMX	magnetic graphitized biochar (GMBC)	0.06	10	3	5.04	60	99.4	Four times	23.1	[143]
	nitrogen-doped biochar from pomelo peel	0.1	10	0.5	7	30	95	Four times	80	[144]
ACT	nanoscale zero-valent iron biochar (BC-Fe^0) derived from waste lignocellulose rice	0.5	10	1.8	7	20	100	Five times	93.8	[92]
	cobalt-impregnated biochar produced from CO_2-mediated pyrolysis of Co/lignin	0.05	5	0.3	7	30	90	Four times	90	[91]
CPX	the magnetic biochar (Fe2O3@LBC) derived from loofah	0.4	10	0.4	7	200	73.9	Four times	50	[64]
LEV	innovative magnetic $MgFe_2O_4$/BC (MMB) derived from pomelo peel	0.4	10	4.2	5	240	87.87	Three times	67.9	[145]
	Co@RBC prepared from cobalt nanoparticles embedded in biochar	0.2	10	0.5	4.5	10	100	Five times	100	[65]

Table 5. The removal of five major pollutants by biochar through adsorption.

Target Pollutants	Adsorbent	Adsorbent Dosage (g/L)	Pollutant Concentration (mg/L)	pH	Time	Adsorption Capacity (mg/g)	Regeneration	Cycle Times	Last Adsorption Capacity (mg/g)	Ref.
TC	pyrolyzed sludge biochar	0.2	20	7	24 h	54.8	NaOH, ethanol, and thermal treatment	Four times	35.4 (NaOH treatment) 49.8 (thermal treatment)	[146]
	tea residue-based biochar	1	100	2	360 min	70.8	Ethanol treatment	Five times	42.6	[70]
SMX	$FeCl_3$-activated bermudagrass (BG)-derived biochar (IA-BCs)	10	100	3	48 h	280	NaOH desorption, thermal oxidation, and Fenton oxidation	Four times	151.2 (NaOH treatment) 128.8 (thermal treatment)	[147]
	Fe-impregnated graphited biochar	0.2	50	5	240 min	187.31	NaOH treatment	Three times	34.85	[148]
ACT	ZnAl/biochar	0.1	125	5	180 min	1108.43	NaOH treatment	Three times	332.5	[63]
CPX	anthriscus sylvestris-derived activated biochar	0.1	30	4	24 h	384.31	NaOH treatment	Three times	115.3	[93]
LEV	biochar-supported $MgFe_2O_4$ (BMF)	0.3	100	5	1400 min	44.9	NaOH treatment	Four times	33.3	[102]

5.2. Future Prospects

The application of biochar in the field of removing pharmaceutical pollutants still have many challenges. According to the current research status, the future research and prospects are listed as follows (Figure 9).

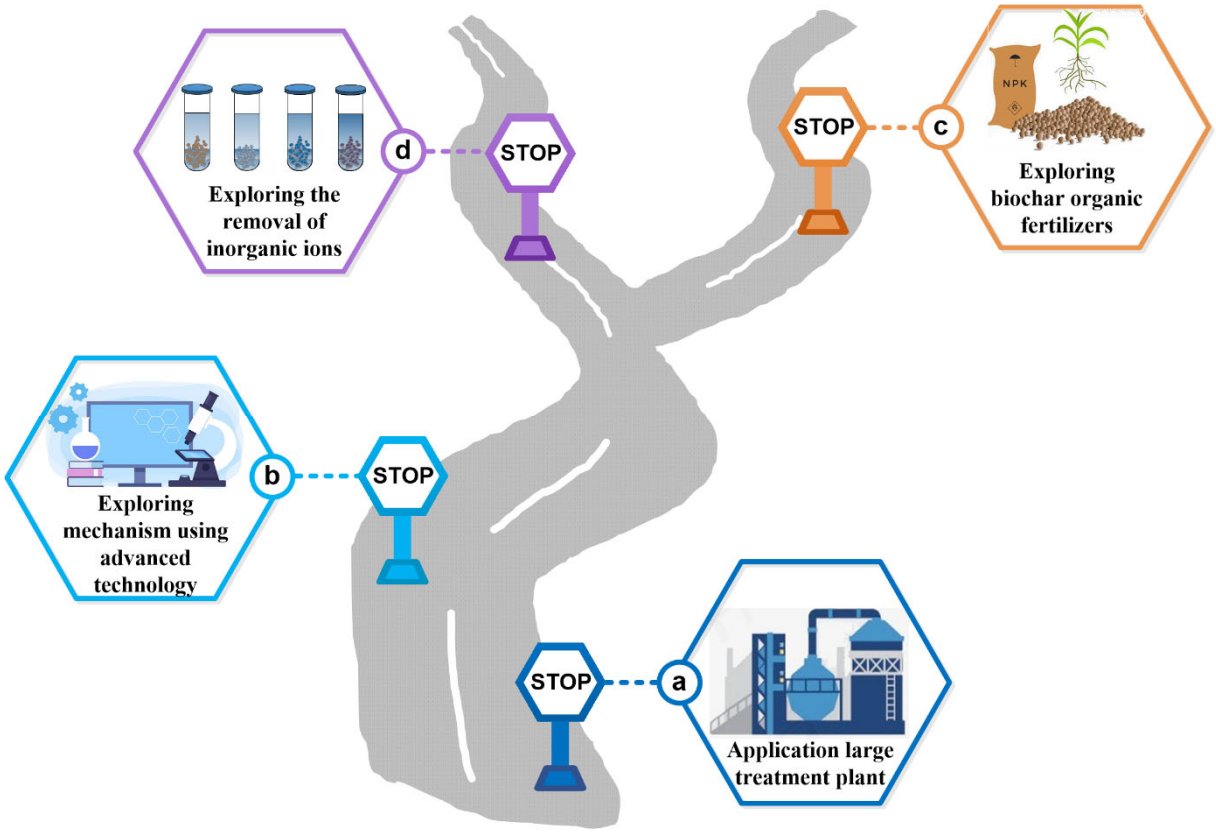

Figure 9. Schematic diagram of improving prospects of biochar in water treatment.

(I) The current research on the persulfate oxidation method is mainly concentrated on the laboratory scale, and there is a lack of research on large-scale actual water bodies. Changes in pH and the generation of secondary by-products must be comprehensively considered before practical applications. Moreover, a higher concentration of persulfate must be used in the treatment of pharmaceutical pollutants, which will result in a large amount of sulfate ions remaining in the aquatic environment. The separation of sulfates in the removal of pharmaceutical pollutants has adverse effects on the environment. Therefore, it is also worth exploring how to limit the dose of persulfate and how to restore persulfate in situ.

(II) There are relatively few studies on the catalytic mechanism of biochar/persulfate-AOPs, and the degradation pathways generated by persulfate activation are diverse. According to the material properties, such as the surface functional groups, the presence of metals, oxygen vacancies, or other defects, they may involve the simultaneous generation of free-radical and non-radical pathways. There is no precise rule of thumb for forecasting either pathway. Using advanced characterization techniques, it is expected that the active surface sites of catalysts will be determined by measuring the surface changes before and after the reaction. The sample preparation for characterization may lead to changes in the catalyst surface, and in situ measurement should be considered in future research. In addition, density functional theory can be used as a useful tool to explore the reaction mechanism at the molecular level.

(III) Biochar can also be used to remediate and improve soils, helping to maintain environmental sustainability. Composting organic waste with biochar can promote the

biodegradation of organic waste. But for different organic wastes and different types of biochar, different doses of biochar are required. Therefore, an appropriate biochar application strategy should be developed according to the characteristics of organic waste, compost, and soil.

(IV) The technology of applying biochar to treat pharmaceutical pollutants can be applied to remove other types of pollutants to improve the aquatic environment. Neither pristine biochar nor even biochar composites have been shown to improve the adsorption of nutrients such as phosphate and nitrate in water, which are the main compounds that pollute freshwater ecosystems and cause eutrophication. Therefore, further research is required to develop or identify a suitable material to control these substances.

Author Contributions: Conceptualization, Z.K., X.J., Y.Z. and Z.H.; writing—original draft preparation, Z.K.; writing—review and editing, Z.K., X.J., Y.Z. and X.K.; visualization, X.K., M.G. and Z.H.; supervision, D.L., C.W. and Z.H.; project administration, C.W. and Z.H.; funding acquisition, Z.H. All authors have read and agreed to the published version of the manuscript.

Funding: This work was funded by the Hebei National Science Fund for Distinguished Young Scholars (No. E2019209433), Youth Talent Program of Department of Education of Hebei Province (No. BJ2018020) and Hebei Province High-level Talents Funded Project (No. B2020003030).

Institutional Review Board Statement: Not applicable.

Informed Consent Statement: Not applicable.

Conflicts of Interest: The authors declare no conflict of interest.

References

1. Tang, F.; He, T.; Zhang, H.; Wu, X.; Li, Y.; Long, F.; Xiang, Y.; Zhu, L.; Wu, J.; Wu, X. The MnO@N-doped carbon composite derived from electrospinning as cathode material for aqueous zinc ion battery. *J. Electroanal. Chem.* **2020**, *873*, 114368. [CrossRef]
2. Li, B.; Xue, J.; Han, C.; Liu, N.; Ma, K.; Zhang, R.; Wu, X.; Dai, L.; Wang, L.; He, Z. A hafnium oxide-coated dendrite-free zinc anode for rechargeable aqueous zinc-ion batteries. *J. Colloid Interface Sci.* **2021**, *599*, 467–475. [CrossRef] [PubMed]
3. Jiang, Y.; Liu, Z.; Lv, Y.; Tang, A.; Dai, L.; Wang, L.; He, Z. Perovskite enables high performance vanadium redox flow battery. *Chem. Eng. J.* **2022**, *443*, 136341. [CrossRef]
4. Xiang, Y.; Huang, M.; Jiang, Y.; Liu, S.; Li, J.; Wu, J.; Liu, Z.; Zhu, L.; Wu, X.; He, Z.; et al. Ionic liquid assisted hydrothermal synthesis of $0.5Li_2MnO_3{\cdot}0.5LiNi_{0.5}Mn_{0.5}O_2$ for lithium ion batteries. *J. Alloys Compd.* **2021**, *864*, 158177. [CrossRef]
5. Kong, P.; Zhu, L.; Li, F.; Xu, G. Self-Supporting Electrode Composed of SnSe Nanosheets, Thermally Treated Protein, and Reduced Graphene Oxide with Enhanced Pseudocapacitance for Advanced Sodium-Ion Batteries. *ChemElectroChem* **2019**, *6*, 5642–5650. [CrossRef]
6. Jiang, Z.; Li, Y.; Han, C.; Huang, Z.; Wu, X.; He, Z.; Meng, W.; Dai, L.; Wang, L. Raising Lithium Storage Performances of $NaTi_2(PO_4)_3$ by Nitrogen and Sulfur Dual-Doped Carbon Layer. *J. Electrochem. Soc.* **2020**, *167*, 20550. [CrossRef]
7. Chen, G.; Yu, Y.; Liang, L.; Duan, X.; Li, R.; Lu, X.; Yan, B.; Li, N.; Wang, S. Remediation of antibiotic wastewater by coupled photocatalytic and persulfate oxidation system: A critical review. *J. Hazard. Mater.* **2021**, *408*, 124461. [CrossRef]
8. Ferrer-Polonio, E.; Fernandez-Navarro, J.; Iborra-Clar, M.I.; Alcaina-Miranda, M.I.; Mendoza-Roca, J.A. Removal of pharmaceutical compounds commonly-found in wastewater through a hybrid biological and adsorption process. *J. Environ. Manag.* **2020**, *263*, 110368. [CrossRef]
9. Zhu, T.-T.; Su, Z.-X.; Lai, W.-X.; Zhang, Y.-B.; Liu, Y.-W. Insights into the fate and removal of antibiotics and antibiotic resistance genes using biological wastewater treatment technology. *Sci. Total Environ.* **2021**, *776*, 145906. [CrossRef]
10. Igwegbe, C.A.; Aniagor, C.O.; Oba, S.N.; Yap, P.-S.; Iwuchukwu, F.U.; Liu, T.; de Souza, E.C.; Ighalo, J.O. Environmental protection by the adsorptive elimination of acetaminophen from water: A comprehensive review. *J. Ind. Eng. Chem.* **2021**, *104*, 117–135. [CrossRef]
11. Yi, X.; Tran, N.H.; Yin, T.; He, Y.; Gin, K.Y. Removal of selected PPCPs, EDCs, and antibiotic resistance genes in landfill leachate by a full-scale constructed wetlands system. *Water Res.* **2017**, *121*, 46–60. [CrossRef]
12. Szymańska, U.; Wiergowski, M.; Sołtyszewski, I.; Kuzemko, J.; Wiergowska, G.; Woźniak, M.K. Presence of antibiotics in the aquatic environment in Europe and their analytical monitoring: Recent trends and perspectives. *Microchem. J.* **2019**, *147*, 729–740. [CrossRef]
13. Xu, W.; Zou, R.; Jin, B.; Zhang, G.; Su, Y.; Zhang, Y. The ins and outs of pharmaceutical wastewater treatment by microbial electrochemical technologies. *Sustain. Horiz.* **2022**, *1*, 100003. [CrossRef]
14. Feng, L.; Li, X.; Chen, X.; Huang, Y.; Peng, K.; Huang, Y.; Yan, Y.; Chen, Y. Pig manure-derived nitrogen-doped mesoporous carbon for adsorption and catalytic oxidation of tetracycline. *Sci. Total Environ.* **2020**, *708*, 135071. [CrossRef]

15. Zungu, V.; Hadebe, L.; Mpungose, P.; Hamza, I.; Amaku, J.; Gumbi, B. Fabrication of Biochar Materials from Biowaste Coffee Grounds and Assessment of Its Adsorbent Efficiency for Remediation of Water-Soluble Pharmaceuticals. *Sustainability* **2022**, *14*, 2931. [CrossRef]
16. Priyadarshini, M.; Das, I.; Ghangrekar, M.M.; Blaney, L. Advanced oxidation processes: Performance, advantages, and scale-up of emerging technologies. *J. Environ. Manag.* **2022**, *316*, 115295. [CrossRef]
17. Wang, C.; Huang, R.; Sun, R.; Yang, J.; Sillanpää, M. A review on persulfates activation by functional biochar for organic contaminants removal: Synthesis, characterizations, radical determination, and mechanism. *J. Environ. Chem. Eng.* **2021**, *9*, 106267. [CrossRef]
18. Liang, J.; Xu, X.; Qamar Zaman, W.; Hu, X.; Zhao, L.; Qiu, H.; Cao, X. Different mechanisms between biochar and activated carbon for the persulfate catalytic degradation of sulfamethoxazole: Roles of radicals in solution or solid phase. *Chem. Eng. J.* **2019**, *375*, 121908. [CrossRef]
19. Zhao, Y.; Dai, H.; Ji, J.; Yuan, X.; Li, X.; Jiang, L.; Wang, H. Resource utilization of luffa sponge to produce biochar for effective degradation of organic contaminants through persulfate activation. *Sep. Purif. Technol.* **2022**, *288*, 120650. [CrossRef]
20. Li, J.; Liu, G.; Liu, B.; Min, Z.; Qian, D.; Jiang, J.; Li, J. Fe-doped CoSe2 nanoparticles encapsulated in N-doped bamboo-like carbon nanotubes as an efficient electrocatalyst for oxygen evolution reaction. *Electrochim. Acta* **2018**, *265*, 577–585. [CrossRef]
21. Li, J.; Jiang, J.; Zhao, D.; Xu, Z.; Liu, M.; Liu, X.; Tong, H.; Qian, D. Novel hierarchical sea urchin-like Prussian blue@palladium core–shell heterostructures supported on nitrogen-doped reduced graphene oxide: Facile synthesis and excellent guanine sensing performance. *Electrochim. Acta* **2020**, *330*, 135196. [CrossRef]
22. Wang, C.; Luo, D.; Zhang, X.; Huang, R.; Cao, Y.; Liu, G.; Zhang, Y.; Wang, H. Biochar-based slow-release of fertilizers for sustainable agriculture: A mini review. *Environ. Sci. Ecotechnol.* **2022**, *10*, 100167. [CrossRef]
23. Selvarajoo, A.; Wong, Y.L.; Khoo, K.S.; Chen, W.H.; Show, P.L. Biochar production via pyrolysis of citrus peel fruit waste as a potential usage as solid biofuel. *Chemosphere* **2022**, *294*, 133671. [CrossRef]
24. Irshad, M.K.; Ibrahim, M.; Noman, A.; Shang, J.; Mahmood, A.; Mubashir, M.; Khoo, K.S.; Ng, H.S.; Show, P.L. Elucidating the impact of goethite-modified biochar on arsenic mobility, bioaccumulation in paddy rice (*Oryza sativa* L.) along with soil enzyme activities. *Process. Saf. Environ. Prot.* **2022**, *160*, 958–967. [CrossRef]
25. Wang, C.; Sun, R.; Huang, R. Highly dispersed iron-doped biochar derived from sawdust for Fenton-like degradation of toxic dyes. *J. Clean. Prod.* **2021**, *297*, 126681. [CrossRef]
26. Zhang, X.; Gang, D.D.; Zhang, J.; Lei, X.; Lian, Q.; Holmes, W.E.; Zappi, M.E.; Yao, H. Insight into the activation mechanisms of biochar by boric acid and its application for the removal of sulfamethoxazole. *J. Hazard. Mater.* **2022**, *424*, 127333. [CrossRef]
27. Fang, G.; Wu, W.; Liu, C.; Dionysiou, D.D.; Deng, Y.; Zhou, D. Activation of persulfate with vanadium species for PCBs degradation: A mechanistic study. *Appl. Catal. B* **2017**, *202*, 1–11. [CrossRef]
28. Ahmad, M.; Rajapaksha, A.U.; Lim, J.E.; Zhang, M.; Bolan, N.; Mohan, D.; Vithanage, M.; Lee, S.S.; Ok, Y.S. Biochar as a sorbent for contaminant management in soil and water: A review. *Chemosphere* **2014**, *99*, 19–33. [CrossRef] [PubMed]
29. Xiang, Y.; Xu, Z.; Zhou, Y.; Wei, Y.; Long, X.; He, Y.; Zhi, D.; Yang, J.; Luo, L. A sustainable ferromanganese biochar adsorbent for effective levofloxacin removal from aqueous medium. *Chemosphere* **2019**, *237*, 124464. [CrossRef] [PubMed]
30. Xi, M.; Cui, K.; Cui, M.; Ding, Y.; Guo, Z.; Chen, Y.; Li, C.; Li, X. Enhanced norfloxacin degradation by iron and nitrogen co-doped biochar: Revealing the radical and nonradical co-dominant mechanism of persulfate activation. *Chem. Eng. J.* **2021**, *420*, 129902. [CrossRef]
31. Wang, B.-h.; Zhang, Q.; Hong, J.-m. Fe0/C-bentonite alginate beads and oyster shell fixed-bed column combined process to continuously remove N-acetyl-p-aminophenol in persulfate system. *J. Ind. Eng. Chem.* **2018**, *67*, 301–311. [CrossRef]
32. Pi, Z.; Li, X.; Wang, D.; Xu, Q.; Tao, Z.; Huang, X.; Yao, F.; Wu, Y.; He, L.; Yang, Q. Persulfate activation by oxidation biochar supported magnetite particles for tetracycline removal: Performance and degradation pathway. *J. Clean. Prod.* **2019**, *235*, 1103–1115. [CrossRef]
33. Ledjeri, A.; Yahiaoui, I.; Kadji, H.; Aissani-Benissad, F.; Amrane, A.; Fourcade, F. Combination of the Electro/Fe^{3+}/peroxydisulfate (PDS) process with activated sludge culture for the degradation of sulfamethazine. *Environ. Toxicol. Pharmacol.* **2017**, *53*, 34–39. [CrossRef]
34. Kim, D.-G.; Ko, S.-O. Effects of thermal modification of a biochar on persulfate activation and mechanisms of catalytic degradation of a pharmaceutical. *Chem. Eng. J.* **2020**, *399*, 125377. [CrossRef]
35. Kemmou, L.; Frontistis, Z.; Vakros, J.; Manariotis, I.D.; Mantzavinos, D. Degradation of antibiotic sulfamethoxazole by biochar-activated persulfate: Factors affecting the activation and degradation processes. *Catal. Today* **2018**, *313*, 128–133. [CrossRef]
36. Hu, Y.; Chen, D.; Zhang, R.; Ding, Y.; Ren, Z.; Fu, M.; Cao, X.; Zeng, G. Singlet oxygen-dominated activation of peroxymonosulfate by passion fruit shell derived biochar for catalytic degradation of tetracycline through a non-radical oxidation pathway. *J. Hazard. Mater.* **2021**, *419*, 126495. [CrossRef]
37. He, L.; Yang, S.; Shen, S.; Ma, Y.; Chen, Y.; Xue, J.; Wang, J.; Zheng, L.; Wu, L.; Zhang, Z.; et al. Novel insights into the mechanism of periodate activation by heterogeneous ultrasonic-enhanced sludge biochar: Relevance for efficient degradation of levofloxacin. *J. Hazard. Mater.* **2022**, *434*, 128860. [CrossRef]
38. Gholami, P.; Khataee, A.; Soltani, R.D.C.; Dinpazhoh, L.; Bhatnagar, A. Photocatalytic degradation of gemifloxacin antibiotic using Zn-Co-LDH@biochar nanocomposite. *J. Hazard. Mater.* **2020**, *382*, 121070. [CrossRef]

39. Ahmed, M.J.; Hameed, B.H. Removal of emerging pharmaceutical contaminants by adsorption in a fixed-bed column: A review. *Ecotoxicol. Environ. Saf.* **2018**, *149*, 257–266. [CrossRef]
40. Wang, J.; Wang, Z.; Liang, J.; He, Z. Electrolysis-assisted recovery of reverse-fluxed solutes in forward osmosis. *Desalination* **2021**, *520*, 115346. [CrossRef]
41. Xing, H.; Hu, P.; Li, S.; Zuo, Y.; Han, J.; Hua, X.; Wang, K.; Yang, F.; Feng, P.; Chang, T. Adsorption and diffusion of oxygen on metal surfaces studied by first-principle study: A review. *J. Mater. Sci. Technol.* **2021**, *62*, 180–194. [CrossRef]
42. Sun, D.; Li, F.; Jin, J.; Khan, S.; Eltohamy, K.M.; He, M.; Liang, X. Qualitative and quantitative investigation on adsorption mechanisms of Cd(II) on modified biochar derived from co-pyrolysis of straw and sodium phytate. *Sci. Total Environ.* **2022**, *829*, 154599. [CrossRef]
43. Barquilha, C.E.R.; Braga, M.C.B. Adsorption of organic and inorganic pollutants onto biochars: Challenges, operating conditions, and mechanisms. *Bioresour. Technol. Rep.* **2021**, *15*, 100728. [CrossRef]
44. Cheng, G.; Tan, B.; Zhang, Z.; Fu, S.; Haiyan, W.; Wang, F. Characteristics of coal-oxygen chemisorption at the low-temperature oxidation stage: DFT and experimental study. *Fuel* **2022**, *315*, 123120. [CrossRef]
45. Liu, N.; Yu, F.; Wang, Y.; Ma, J. Effects of environmental aging on the adsorption behavior of antibiotics from aqueous solutions in microplastic-graphene coexisting systems. *Sci. Total Environ.* **2022**, *806*, 150956. [CrossRef]
46. Guo, R.; Xi, B.; Guo, C.; Cheng, X.; Lv, N.; Liu, W.; Borthwick, A.G.L.; Xu, J. Persulfate-based advanced oxidation processes: The new hope brought by nanocatalyst immobilization. *Environ. Funct. Mater.* **2022**, *1*, 67–91. [CrossRef]
47. Tian, K.; Hu, L.; Li, L.; Zheng, Q.; Xin, Y.; Zhang, G. Recent advances in persulfate-based advanced oxidation processes for organic wastewater treatment. *Chin. Chem. Lett.* **2022**, *33*, 4461–4477. [CrossRef]
48. Feng, Y.; Liu, J.; Wu, D.; Zhou, Z.; Deng, Y.; Zhang, T.; Shih, K. Efficient degradation of sulfamethazine with $CuCo_2O_4$ spinel nanocatalysts for peroxymonosulfate activation. *Chem. Eng. J.* **2015**, *280*, 514–524. [CrossRef]
49. Luo, R.; Li, M.; Wang, C.; Zhang, M.; Nasir Khan, M.A.; Sun, X.; Shen, J.; Han, W.; Wang, L.; Li, J. Singlet oxygen-dominated non-radical oxidation process for efficient degradation of bisphenol A under high salinity condition. *Water Res.* **2019**, *148*, 416–424. [CrossRef] [PubMed]
50. Xiao, P.-f.; An, L.; Wu, D.-d. The use of carbon materials in persulfate-based advanced oxidation processes: A review. *New Carbon Mater.* **2020**, *35*, 667–683. [CrossRef]
51. Liu, B.; Guo, W.; Wang, H.; Si, Q.; Zhao, Q.; Luo, H.; Ren, N. Activation of peroxymonosulfate by cobalt-impregnated biochar for atrazine degradation: The pivotal roles of persistent free radicals and ecotoxicity assessment. *J. Hazard. Mater.* **2020**, *398*, 122768. [CrossRef]
52. Huang, R.; Yang, J.; Cao, Y.; Dionysiou, D.D.; Wang, C. Peroxymonosulfate catalytic degradation of persistent organic pollutants by engineered catalyst of self-doped iron/carbon nanocomposite derived from waste toner powder. *Sep. Purif. Technol.* **2022**, *291*, 120963. [CrossRef]
53. Ioannidi, A.; Oulego, P.; Collado, S.; Petala, A.; Arniella, V.; Frontistis, Z.; Angelopoulos, G.N.; Diaz, M.; Mantzavinos, D. Persulfate activation by modified red mud for the oxidation of antibiotic sulfamethoxazole in water. *J. Environ. Manag.* **2020**, *270*, 110820. [CrossRef]
54. Li, J.; Zhu, J.; Fang, L.; Nie, Y.; Tian, N.; Tian, X.; Lu, L.; Zhou, Z.; Yang, C.; Li, Y. Enhanced peroxymonosulfate activation by supported microporous carbon for degradation of tetracycline via non-radical mechanism. *Sep. Purif. Technol.* **2020**, *240*, 116617. [CrossRef]
55. Fu, H.; Zhao, P.; Xu, S.; Cheng, G.; Li, Z.; Li, Y.; Li, K.; Ma, S. Fabrication of Fe_3O_4 and graphitized porous biochar composites for activating peroxymonosulfate to degrade p-hydroxybenzoic acid: Insights on the mechanism. *Chem. Eng. J.* **2019**, *375*, 121980. [CrossRef]
56. Al-Othman, Z.A.; Ali, R.; Naushad, M. Hexavalent chromium removal from aqueous medium by activated carbon prepared from peanut shell: Adsorption kinetics, equilibrium and thermodynamic studies. *Chem. Eng. J.* **2012**, *184*, 238–247. [CrossRef]
57. Fu, Y.; Shen, Y.; Zhang, Z.; Ge, X.; Chen, M. Activated bio-chars derived from rice husk via one- and two-step KOH-catalyzed pyrolysis for phenol adsorption. *Sci. Total Environ.* **2019**, *646*, 1567–1577. [CrossRef]
58. Xia, D.; Tan, F.; Zhang, C.; Jiang, X.; Chen, Z.; Li, H.; Zheng, Y.; Li, Q.; Wang, Y. $ZnCl_2$-activated biochar from biogas residue facilitates aqueous As(III) removal. *Appl. Surf. Sci.* **2016**, *377*, 361–369. [CrossRef]
59. Ye, S.; Xiong, W.; Liang, J.; Yang, H.; Wu, H.; Zhou, C.; Du, L.; Guo, J.; Wang, W.; Xiang, L.; et al. Refined regulation and nitrogen doping of biochar derived from ramie fiber by deep eutectic solvents (DESs) for catalytic persulfate activation toward non-radical organics degradation and disinfection. *J. Colloid Interface Sci.* **2021**, *601*, 544–555. [CrossRef]
60. Sun, F.; Chen, T.; Liu, H.; Zou, X.; Zhai, P.; Chu, Z.; Shu, D.; Wang, H.; Chen, D. The pH-dependent degradation of sulfadiazine using natural siderite activating PDS: The role of singlet oxygen. *Sci. Total Environ.* **2021**, *784*, 147117. [CrossRef]
61. Sun, C.; Chen, T.; Huang, Q.; Duan, X.; Zhan, M.; Ji, L.; Li, X.; Yan, J. Selective production of singlet oxygen from zinc-etching hierarchically porous biochar for sulfamethoxazole degradation. *Environ. Pollut.* **2021**, *290*, 117991. [CrossRef]
62. Yin, R.; Guo, W.; Wang, H.; Du, J.; Wu, Q.; Chang, J.-S.; Ren, N. Singlet oxygen-dominated peroxydisulfate activation by sludge-derived biochar for sulfamethoxazole degradation through a nonradical oxidation pathway: Performance and mechanism. *Chem. Eng. J.* **2019**, *357*, 589–599. [CrossRef]

63. Moreno-Pérez, J.; Pauletto, P.S.; Cunha, A.M.; Bonilla-Petriciolet, Á.; Salau, N.P.G.; Dotto, G.L. Three-dimensional mass transport modeling of pharmaceuticals adsorption inside ZnAl/biochar composite. *Colloids Surf. A Physicochem. Eng. Asp.* **2021**, *614*, 126170. [CrossRef]
64. Song, H.; Li, Q.; Ye, Y.; Pan, F.; Zhang, D.; Xia, D. Degradation of cephalexin by persulfate activated with magnetic loofah biochar: Performance and mechanism. *Sep. Purif. Technol.* **2021**, *272*, 118971. [CrossRef]
65. Liu, J.; Jiang, J.; Wang, M.; Kang, J.; Zhang, J.; Liu, S.; Tang, Y.; Li, S. Peroxymonosulfate activation by cobalt particles embedded into biochar for levofloxacin degradation: Efficiency, stability, and mechanism. *Sep. Purif. Technol.* **2022**, *294*, 121082. [CrossRef]
66. Liu, J.; Zhou, B.; Zhang, H.; Ma, J.; Mu, B.; Zhang, W. A novel Biochar modified by Chitosan-Fe/S for tetracycline adsorption and studies on site energy distribution. *Bioresour. Technol.* **2019**, *294*, 122152. [CrossRef] [PubMed]
67. Li, X.; Xu, J.; Shi, J.; Luo, X. Rapid and efficient adsorption of tetracycline from aqueous solution in a wide pH range by using iron and aminoacetic acid sequentially modified hierarchical porous biochar. *Bioresour. Technol.* **2022**, *346*, 126672. [CrossRef] [PubMed]
68. Sheng, X.; Wang, J.; Cui, Q.; Zhang, W.; Zhu, X. A feasible biochar derived from biogas residue and its application in the efficient adsorption of tetracycline from an aqueous solution. *Environ. Res.* **2022**, *207*, 112175. [CrossRef] [PubMed]
69. Zhang, X.; Li, Y.; Wu, M.; Pang, Y.; Hao, Z.; Hu, M.; Qiu, R.; Chen, Z. Enhanced adsorption of tetracycline by an iron and manganese oxides loaded biochar: Kinetics, mechanism and column adsorption. *Bioresour. Technol.* **2021**, *320*, 124264. [CrossRef] [PubMed]
70. Mu, Y.; He, W.; Ma, H. Enhanced adsorption of tetracycline by the modified tea-based biochar with the developed mesoporous and surface alkalinity. *Bioresour. Technol.* **2021**, *342*, 126001. [CrossRef]
71. Liu, Q.; Li, D.; Cheng, H.; Cheng, J.; Du, K.; Hu, Y.; Chen, Y. High mesoporosity phosphorus-containing biochar fabricated from Camellia oleifera shells: Impressive tetracycline adsorption performance and promotion of pyrophosphate-like surface functional groups (C-O-P bond). *Bioresour. Technol.* **2021**, *329*, 124922. [CrossRef]
72. Wang, C.; Sun, R.; Huang, R.; Wang, H. Superior fenton-like degradation of tetracycline by iron loaded graphitic carbon derived from microplastics: Synthesis, catalytic performance, and mechanism. *Sep. Purif. Technol.* **2021**, *270*, 118773. [CrossRef]
73. Kang, X.; Jia, X.; Kang, Z.; Zhang, Y.; Zhang, D.; Wei, J.; Guo, A.; Ge, M.; He, Z. Activation of peroxydisulfate by black fungus-derived N-doped biochar for tetracycline degradation via non-radical dominated oxidation pathway. *Surf. Interfaces* **2022**, *31*, 102007. [CrossRef]
74. Gao, Y.; Wang, Q.; Ji, G.; Li, A. Degradation of antibiotic pollutants by persulfate activated with various carbon materials. *Chem. Eng. J.* **2022**, *429*, 132387. [CrossRef]
75. Ji, L.; Chen, W.; Zheng, S.; Xu, Z.; Zhu, D. Adsorption of sulfonamide antibiotics to multiwalled carbon nanotubes. *Langmuir* **2009**, *25*, 11608–11613. [CrossRef]
76. Ahmed, M.B.; Zhou, J.L.; Ngo, H.H.; Guo, W.; Johir, M.A.H.; Sornalingam, K. Single and competitive sorption properties and mechanism of functionalized biochar for removing sulfonamide antibiotics from water. *Chem. Eng. J.* **2017**, *311*, 348–358. [CrossRef]
77. Yang, W.; Lu, Y.; Zheng, F.; Xue, X.; Li, N.; Liu, D. Adsorption behavior and mechanisms of norfloxacin onto porous resins and carbon nanotube. *Chem. Eng. J.* **2012**, *179*, 112–118. [CrossRef]
78. Reguyal, F.; Sarmah, A.K.; Gao, W. Synthesis of magnetic biochar from pine sawdust via oxidative hydrolysis of $FeCl_2$ for the removal sulfamethoxazole from aqueous solution. *J. Hazard. Mater.* **2017**, *321*, 868–878. [CrossRef]
79. Reguyal, F.; Sarmah, A.K. Adsorption of sulfamethoxazole by magnetic biochar: Effects of pH, ionic strength, natural organic matter and 17alpha-ethinylestradiol. *Sci. Total Environ.* **2018**, *628–629*, 722–730. [CrossRef]
80. Du, L.; Xu, W.; Liu, S.; Li, X.; Huang, D.; Tan, X.; Liu, Y. Activation of persulfate by graphitized biochar for sulfamethoxazole removal: The roles of graphitic carbon structure and carbonyl group. *J. Colloid Interface Sci.* **2020**, *577*, 419–430. [CrossRef]
81. Qi, Y.; Ge, B.; Zhang, Y.; Jiang, B.; Wang, C.; Akram, M.; Xu, X. Three-dimensional porous graphene-like biochar derived from Enteromorpha as a persulfate activator for sulfamethoxazole degradation: Role of graphitic N and radicals transformation. *J. Hazard. Mater.* **2020**, *399*, 123039. [CrossRef]
82. Ji, Y.; Fan, Y.; Liu, K.; Kong, D.; Lu, J. Thermo activated persulfate oxidation of antibiotic sulfamethoxazole and structurally related compounds. *Water Res.* **2015**, *87*, 1–9. [CrossRef]
83. Gao, S.; Zhao, Z.; Xu, Y.; Tian, J.; Qi, H.; Lin, W.; Cui, F. Oxidation of sulfamethoxazole (SMX) by chlorine, ozone and permanganate—A comparative study. *J. Hazard. Mater.* **2014**, *274*, 258–269. [CrossRef]
84. Liu, L.; Lin, S.; Zhang, W.; Farooq, U.; Shen, G.; Hu, S. Kinetic and mechanistic investigations of the degradation of sulfachloropyridazine in heat-activated persulfate oxidation process. *Chem. Eng. J.* **2018**, *346*, 515–524. [CrossRef]
85. Lim, S.; Kim, J.H.; Park, H.; Kwak, C.; Yang, J.; Kim, J.; Ryu, S.Y.; Lee, J. Role of electrostatic interactions in the adsorption of dye molecules by Ti3C2-MXenes. *RSC Adv.* **2021**, *11*, 6201–6211. [CrossRef] [PubMed]
86. Boudrahem, N.; Delpeux-Ouldriane, S.; Khenniche, L.; Boudrahem, F.; Aissani-Benissad, F.; Gineys, M. Single and mixture adsorption of clofibric acid, tetracycline and paracetamol onto Activated carbon developed from cotton cloth residue. *Process. Saf. Environ. Prot.* **2017**, *111*, 544–559. [CrossRef]
87. Zhou, X.; Lai, C.; Liu, S.; Li, B.; Qin, L.; Liu, X.; Yi, H.; Fu, Y.; Li, L.; Zhang, M.; et al. Activation of persulfate by swine bone derived biochar: Insight into the specific role of different active sites and the toxicity of acetaminophen degradation pathways. *Sci. Total Environ.* **2022**, *807*, 151059. [CrossRef] [PubMed]

88. Li, J.; Ye, Q.; Gan, J. Degradation and transformation products of acetaminophen in soil. *Water Res.* **2014**, *49*, 44–52. [CrossRef]
89. Wang, J.; Wang, S. Reactive species in advanced oxidation processes: Formation, identification and reaction mechanism. *Chem. Eng. J.* **2020**, *401*, 126158. [CrossRef]
90. Villota, N.; Lomas, J.M.; Camarero, L.M. Study of the paracetamol degradation pathway that generates color and turbidity in oxidized wastewaters by photo-Fenton technology. *J. Photochem. Photobiol. A* **2016**, *329*, 113–119. [CrossRef]
91. Yang, M.T.; Du, Y.; Tong, W.C.; Yip, A.C.K.; Lin, K.A. Cobalt-impregnated biochar produced from CO_2-mediated pyrolysis of Co/lignin as an enhanced catalyst for activating peroxymonosulfate to degrade acetaminophen. *Chemosphere* **2019**, *226*, 924–933. [CrossRef]
92. Zhuo, S.-N.; Ren, H.-Y.; Cao, G.-L.; Xie, G.-J.; Xing, D.-F.; Ren, N.-Q.; Liu, B.-F. Highly efficient activation of persulfate by encapsulated nano-Fe0 biochar for acetaminophen degradation: Rich electron environment and dominant effect of superoxide radical. *Chem. Eng. J.* **2022**, *440*, 135947. [CrossRef]
93. Shirani, Z.; Song, H.; Bhatnagar, A. Efficient removal of diclofenac and cephalexin from aqueous solution using Anthriscus sylvestris-derived activated biochar. *Sci. Total Environ.* **2020**, *745*, 140789. [CrossRef]
94. Al-Gheethi, A.; Noman, E.; Saphira Radin Mohamed, R.M.; Talip, B.; Vo, D.N.; Algaifi, H.A. Cephalexin removal by a novel Cu-Zn bionanocomposite biosynthesized in secondary metabolic products of Aspergillus arenarioides EAN603 with pumpkin peels medium: Optimization, kinetic and artificial neural network models. *J. Hazard. Mater.* **2021**, *419*, 126500. [CrossRef]
95. Naghipour, D.; Amouei, A.; Estaji, M.; Taghavi, K.; Allahabadi, A. Cephalexin adsorption from aqueous solutions by biochar prepared from plantain wood: Equilibrium and kinetics studies. *Desalin. Water Treat.* **2019**, *143*, 374–381. [CrossRef]
96. Ali Noman, E.; Al-Gheethi, A.; Saphira Radin Mohamed, R.M.; Talip, B.A.; Hossain, M.S.; Ali Hamood Altowayti, W.; Ismail, N. Sustainable approaches for removal of cephalexin antibiotic from non-clinical environments: A critical review. *J. Hazard. Mater.* **2021**, *417*, 126040. [CrossRef]
97. Zhang, Y.; Wang, A.; Ren, S.; Wen, Z.; Tian, X.; Li, D.; Li, J. Effect of surface properties of activated carbon fiber cathode on mineralization of antibiotic cefalexin by electro-Fenton and photoelectro-Fenton treatments: Mineralization, kinetics and oxidation products. *Chemosphere* **2019**, *221*, 423–432. [CrossRef]
98. Droguett, C.; Salazar, R.; Brillas, E.; Sires, I.; Carlesi, C.; Marco, J.F.; Thiam, A. Treatment of antibiotic cephalexin by heterogeneous electrochemical Fenton-based processes using chalcopyrite as sustainable catalyst. *Sci. Total Environ.* **2020**, *740*, 140154. [CrossRef]
99. Wang, Z.; Jang, H.M. Comparative study on characteristics and mechanism of levofloxacin adsorption on swine manure biochar. *Bioresour. Technol.* **2022**, *351*, 127025. [CrossRef]
100. Xu, Z.; Xiang, Y.; Zhou, H.; Yang, J.; He, Y.; Zhu, Z.; Zhou, Y. Manganese ferrite modified biochar from vinasse for enhanced adsorption of levofloxacin: Effects and mechanisms. *Environ. Pollut.* **2021**, *272*, 115968. [CrossRef]
101. Xiang, Y.; Yang, X.; Xu, Z.; Hu, W.; Zhou, Y.; Wan, Z.; Yang, Y.; Wei, Y.; Yang, J.; Tsang, D.C.W. Fabrication of sustainable manganese ferrite modified biochar from vinasse for enhanced adsorption of fluoroquinolone antibiotics: Effects and mechanisms. *Sci. Total Environ.* **2020**, *709*, 136079. [CrossRef] [PubMed]
102. Yao, B.; Luo, Z.; Du, S.; Yang, J.; Zhi, D.; Zhou, Y. Sustainable biochar/$MgFe_2O_4$ adsorbent for levofloxacin removal: Adsorption performances and mechanisms. *Bioresour. Technol.* **2021**, *340*, 125698. [CrossRef] [PubMed]
103. Abukhadra, M.R.; Fathallah, W.; El Kashief, F.A.; El-Sherbeeny, A.M.; El-Meligy, M.A.; Awwad, E.M.; Luqman, M. Insight into the antimicrobial and photocatalytic properties of NiO impregnated MCM-48 for effective removal of pathogenic bacteria and toxic levofloxacin residuals. *Microporous Mesoporous Mater.* **2021**, *312*, 110769. [CrossRef]
104. Hu, Z.; Ge, M.; Guo, C. Efficient removal of levofloxacin from different water matrices via simultaneous adsorption and photocatalysis using a magnetic Ag_3PO_4/rGO/$CoFe_2O_4$ catalyst. *Chemosphere* **2021**, *268*, 128834. [CrossRef]
105. Liu, X.; Liu, Y.; Lu, S.; Wang, Z.; Wang, Y.; Zhang, G.; Guo, X.; Guo, W.; Zhang, T.; Xi, B. Degradation difference of ofloxacin and levofloxacin by UV/H_2O_2 and UV/PS (persulfate): Efficiency, factors and mechanism. *Chem. Eng. J.* **2020**, *385*, 123987. [CrossRef]
106. Wen, X.-J.; Niu, C.-G.; Guo, H.; Zhang, L.; Liang, C.; Zeng, G.-M. Photocatalytic degradation of levofloxacin by ternary Ag_2CO_3/CeO_2/AgBr photocatalyst under visible-light irradiation: Degradation pathways, mineralization ability, and an accelerated interfacial charge transfer process study. *J. Catal.* **2018**, *358*, 211–223. [CrossRef]
107. Luo, J.; Yi, Y.; Ying, G.; Fang, Z.; Zhang, Y. Activation of persulfate for highly efficient degradation of metronidazole using Fe(II)-rich potassium doped magnetic biochar. *Sci. Total Environ.* **2022**, *819*, 152089. [CrossRef]
108. Wang, B.; Li, Y.N.; Wang, L. Metal-free activation of persulfates by corn stalk biochar for the degradation of antibiotic norfloxacin: Activation factors and degradation mechanism. *Chemosphere* **2019**, *237*, 124454. [CrossRef]
109. Dong, F.-X.; Yan, L.; Huang, S.-T.; Liang, J.-Y.; Zhang, W.-X.; Yao, X.-W.; Chen, X.; Qian, W.; Guo, P.-R.; Kong, L.-J.; et al. Removal of antibiotics sulfadiazine by a biochar based material activated persulfate oxidation system: Performance, products and mechanism. *Process. Saf. Environ. Prot.* **2022**, *157*, 411–419. [CrossRef]
110. Liang, J.; Xu, X.; Zhong, Q.; Xu, Z.; Zhao, L.; Qiu, H.; Cao, X. Roles of the mineral constituents in sludge-derived biochar in persulfate activation for phenol degradation. *J. Hazard. Mater.* **2020**, *398*, 122861. [CrossRef]
111. Guo, Z.; Zhang, Y.; Gan, S.; He, H.; Cai, N.; Xu, J.; Guo, P.; Chen, B.; Pan, X. Effective degradation of COVID-19 related drugs by biochar-supported red mud catalyst activated persulfate process: Mechanism and pathway. *J. Clean. Prod.* **2022**, *340*, 130753. [CrossRef]
112. Tian, W.; Lin, J.; Zhang, H.; Duan, X.; Sun, H.; Wang, H.; Wang, S. Enhanced removals of micropollutants in binary organic systems by biomass derived porous carbon/peroxymonosulfate. *J. Hazard. Mater.* **2021**, *408*, 124459. [CrossRef]

113. Naima, A.; Ammar, F.; Abdelkader, O.; Rachid, C.; Lynda, H.; Syafiuddin, A.; Boopathy, R. Development of a novel and efficient biochar produced from pepper stem for effective ibuprofen removal. *Bioresour. Technol.* **2022**, *347*, 126685. [CrossRef]
114. Zheng, X.; He, X.; Peng, H.; Wen, J.; Lv, S. Efficient adsorption of ciprofloxacin using Ga_2S_3/S-modified biochar via the high-temperature sulfurization. *Bioresour. Technol.* **2021**, *334*, 125238. [CrossRef]
115. He, X.; Li, J.; Meng, Q.; Guo, Z.; Zhang, H.; Liu, Y. Enhanced adsorption capacity of sulfadiazine on tea waste biochar from aqueous solutions by the two-step sintering method without corrosive activator. *J. Environ. Chem. Eng.* **2021**, *9*, 104898. [CrossRef]
116. Tomul, F.; Arslan, Y.; Kabak, B.; Trak, D.; Kenduzler, E.; Lima, E.C.; Tran, H.N. Peanut shells-derived biochars prepared from different carbonization processes: Comparison of characterization and mechanism of naproxen adsorption in water. *Sci. Total Environ.* **2020**, *726*, 137828. [CrossRef]
117. Escudero-Curiel, S.; Penelas, U.; Sanroman, M.A.; Pazos, M. An approach towards Zero-Waste wastewater technology: Fluoxetine adsorption on biochar and removal by the sulfate radical. *Chemosphere* **2021**, *268*, 129318. [CrossRef]
118. Wang, Q.; Zhang, Z.; Xu, G.; Li, G. Pyrolysis of penicillin fermentation residue and sludge to produce biochar: Antibiotic resistance genes destruction and biochar application in the adsorption of penicillin in water. *J. Hazard. Mater.* **2021**, *413*, 125385. [CrossRef]
119. Chayid, M.A.; Ahmed, M.J. Amoxicillin adsorption on microwave prepared activated carbon from Arundo donax Linn: Isotherms, kinetics, and thermodynamics studies. *J. Environ. Chem. Eng.* **2015**, *3*, 1592–1601. [CrossRef]
120. Ushani, U.; Lu, X.; Wang, J.; Zhang, Z.; Dai, J.; Tan, Y.; Wang, S.; Li, W.; Niu, C.; Cai, T.; et al. Sulfate radicals-based advanced oxidation technology in various environmental remediation: A state-of-the–art review. *Chem. Eng. J.* **2020**, *402*, 126232. [CrossRef]
121. Fan, X.; Li, S.; Sun, M.; Song, C.; Xiao, J.; Du, J.; Tao, P.; Sun, T.; Shao, M.; Wang, T. Degradation of phenol by coal-based carbon membrane integrating sulfate radicals-based advanced oxidation processes. *Ecotoxicol. Environ. Saf.* **2019**, *185*, 109662. [CrossRef]
122. Ersan, M.; Dogan, H. Development of new adsorbents via microwave treatment magnetic PET synthesis from waste PET and investigation of TC removal. *Colloid Interface Sci. Commun.* **2021**, *42*, 100416. [CrossRef]
123. Lemaire, J.; Buès, M.; Kabeche, T.; Hanna, K.; Simonnot, M.-O. Oxidant selection to treat an aged PAH contaminated soil by in situ chemical oxidation. *J. Environ. Chem. Eng.* **2013**, *1*, 1261–1268. [CrossRef]
124. Sun, Y.; Bian, J.; Zhu, Q. Sulfamethoxazole removal of adsorption by carbon—Doped boron nitride in water. *J. Mol. Liq.* **2022**, *349*, 118216. [CrossRef]
125. Yang, D.; Li, J.; Luo, L.; Deng, R.; He, Q.; Chen, Y. Exceptional levofloxacin removal using biochar-derived porous carbon sheets: Mechanisms and density-functional-theory calculation. *Chem. Eng. J.* **2020**, *387*, 124103. [CrossRef]
126. Yu, F.; Li, Y.; Huang, G.; Yang, C.; Chen, C.; Zhou, T.; Zhao, Y.; Ma, J. Adsorption behavior of the antibiotic levofloxacin on microplastics in the presence of different heavy metals in an aqueous solution. *Chemosphere* **2020**, *260*, 127650. [CrossRef]
127. Mahmoud, M.E.; El-Ghanam, A.M.; Mohamed, R.H.A.; Saad, S.R. Enhanced adsorption of Levofloxacin and Ceftriaxone antibiotics from water by assembled composite of nanotitanium oxide/chitosan/nano-bentonite. *Mater. Sci. Eng. C Mater. Biol. Appl.* **2020**, *108*, 110199. [CrossRef] [PubMed]
128. Pan, J.; Bai, X.; Li, Y.; Yang, B.; Yang, P.; Yu, F.; Ma, J. HKUST-1 derived carbon adsorbents for tetracycline removal with excellent adsorption performance. *Environ. Res.* **2022**, *205*, 112425. [CrossRef] [PubMed]
129. Thakur, A.; Sharma, N.; Mann, A. Removal of ofloxacin hydrochloride and paracetamol from aqueous solutions: Binary mixtures and competitive adsorption. *Mater. Today Proc.* **2020**, *28*, 1514–1519. [CrossRef]
130. Li, H.; Tian, J.; Zhu, Z.; Cui, F.; Zhu, Y.-A.; Duan, X.; Wang, S. Magnetic nitrogen-doped nanocarbons for enhanced metal-free catalytic oxidation: Integrated experimental and theoretical investigations for mechanism and application. *Chem. Eng. J.* **2018**, *354*, 507–516. [CrossRef]
131. Yang, S.; Wang, P.; Yang, X.; Shan, L.; Zhang, W.; Shao, X.; Niu, R. Degradation efficiencies of azo dye Acid Orange 7 by the interaction of heat, UV and anions with common oxidants: Persulfate, peroxymonosulfate and hydrogen peroxide. *J. Hazard. Mater.* **2010**, *179*, 552–558. [CrossRef]
132. Geng, G.; Gao, Y.; Zhang, Z.; Gao, K.; Zhang, W.; Song, J. Renewable and robust biomass waste-derived Co-doped carbon aerogels for PMS activation: Catalytic mechanisms and phytotoxicity assessment. *Ecotoxicol. Environ. Saf.* **2021**, *220*, 112381. [CrossRef]
133. Jiang, M.; Lu, J.; Ji, Y.; Kong, D. Bicarbonate-activated persulfate oxidation of acetaminophen. *Water Res.* **2017**, *116*, 324–331. [CrossRef]
134. Liu, J.; Jiang, S.; Chen, D.; Dai, G.; Wei, D.; Shu, Y. Activation of persulfate with biochar for degradation of bisphenol A in soil. *Chem. Eng. J.* **2020**, *381*, 122637. [CrossRef]
135. Peiris, C.; Gunatilake, S.R.; Mlsna, T.E.; Mohan, D.; Vithanage, M. Biochar based removal of antibiotic sulfonamides and tetracyclines in aquatic environments: A critical review. *Bioresour. Technol.* **2017**, *246*, 150–159. [CrossRef]
136. Reza Samarghandi, M.; Tari, K.; Shabanloo, A.; Salari, M.; Zolghadr Nasab, H. Synergistic degradation of acid blue 113 dye in a thermally activated persulfate (TAP)/ZnO-GAC oxidation system: Degradation pathway and application for real textile wastewater. *Sep. Purif. Technol.* **2020**, *247*, 116931. [CrossRef]
137. Mei, Y.; Xu, J.; Zhang, Y.; Li, B.; Fan, S.; Xu, H. Effect of Fe-N modification on the properties of biochars and their adsorption behavior on tetracycline removal from aqueous solution. *Bioresour. Technol.* **2021**, *325*, 124732. [CrossRef]
138. Xiong, S.; Deng, Y.; Gong, D.; Tang, R.; Zheng, J.; Li, L.; Zhou, Z.; Su, L.; Liao, C.; Yang, L. Magnetically modified in-situ N-doped Enteromorpha prolifera derived biochar for peroxydisulfate activation: Electron transfer induced singlet oxygen non-radical pathway. *Chemosphere* **2021**, *284*, 131404. [CrossRef]

139. Miserli, K.; Kogola, D.; Paraschoudi, I.; Konstantinou, I. Activation of persulfate by biochar for the degradation of phenolic compounds in aqueous systems. *Chem. Eng. J. Adv.* **2022**, *9*, 100201. [CrossRef]
140. Wang, H.; Guo, W.; Yin, R.; Du, J.; Wu, Q.; Luo, H.; Liu, B.; Sseguya, F.; Ren, N. Biochar-induced Fe(III) reduction for persulfate activation in sulfamethoxazole degradation: Insight into the electron transfer, radical oxidation and degradation pathways. *Chem. Eng. J.* **2019**, *362*, 561–569. [CrossRef]
141. Li, Q.; Tang, Y.; Zhou, B.; Zhou, J.; Shi, B. Resource utilization of tannery sludge to prepare biochar as persulfate activators for highly efficient degradation of tetracycline. *Bioresour. Technol.* **2022**, *358*, 127417. [CrossRef]
142. Zhong, Q.; Lin, Q.; He, W.; Fu, H.; Huang, Z.; Wang, Y.; Wu, L. Study on the nonradical pathways of nitrogen-doped biochar activating persulfate for tetracycline degradation. *Sep. Purif. Technol.* **2021**, *276*, 119354. [CrossRef]
143. Shen, B.; Liu, Y.; Liu, S.; Tan, X.; Zhang, P.; Du, L.; Wen, J. Catalytic degradation of sulfamethoxazole by persulfate activated with magnetic graphitized biochar: Multiple mechanisms and variables effects. *Process. Saf. Environ. Prot.* **2020**, *144*, 143–157. [CrossRef]
144. Wang, W.; Chen, M. Catalytic degradation of sulfamethoxazole by peroxymonosulfate activation system composed of nitrogen-doped biochar from pomelo peel: Important roles of defects and nitrogen, and detoxification of intermediates. *J. Colloid Interface Sci.* **2022**, *613*, 57–70. [CrossRef]
145. Yao, B.; Luo, Z.; Du, S.; Yang, J.; Zhi, D.; Zhou, Y. Magnetic $MgFe_2O_4$/biochar derived from pomelo peel as a persulfate activator for levofloxacin degradation: Effects and mechanistic consideration. *Bioresour. Technol.* **2022**, *346*, 126547. [CrossRef]
146. Chen, W.; Zhao, B.; Guo, Y.; Guo, Y.; Zheng, Z.; Pak, T.; Li, G. Effect of hydrothermal pretreatment on pyrolyzed sludge biochars for tetracycline adsorption. *J. Environ. Chem. Eng.* **2021**, *9*, 106557. [CrossRef]
147. Zeng, S.; Choi, Y.K.; Kan, E. Iron-activated bermudagrass-derived biochar for adsorption of aqueous sulfamethoxazole: Effects of iron impregnation ratio on biochar properties, adsorption, and regeneration. *Sci. Total Environ.* **2021**, *750*, 141691. [CrossRef]
148. Zhang, R.; Zheng, X.; Chen, B.; Ma, J.; Niu, X.; Zhang, D.; Lin, Z.; Fu, M.; Zhou, S. Enhanced adsorption of sulfamethoxazole from aqueous solution by Fe-impregnated graphited biochar. *J. Clean. Prod.* **2020**, *256*, 120662. [CrossRef]